Review on Underwater Friction Stir Welding of Aluminum Alloys

Vikrant Saumitra*, Yuvraj Singh and Shubham Kumar Ekghara**

Department of Metallurgical and Materials Engineering, Malaviya National Institute of Technology, JLN Marg, Malaviya Nagar, Jaipur

*__Corresponding author:__ Vikrant Saumitra, Department of Metallurgical and Materials Engineering, Malaviya National Institute of Technology, Jaipur, Rajasthan, India, Tel: 8503876621; E-mail: saumitravikrant@gmail.com

Abstract

Underwater friction stir welding is an innovative and novel technique of welding. In this present era, very few researchers and academicians have done research on it. Research on underwater friction stir welding can boost and pave the way for the research area in the field of friction stir welding. Joining using fusion welding processes, results in the formation of solidification defects like porosity, alloy segregation, and hot cracking. To overcome the solidification related problems, solid-state welding processes such as Friction Stir Welding (FSW) prove useful. Though the joining takes place below the melting temperature of the material, the thermal cycle experienced by the Thermo-Mechanical Affected Zone (TMAZ) and Heat Affected Zone (HAZ) is causing grain coarsening and precipitates dissolution, which deteriorates the joint properties resulting in poor mechanical and physical behavior. To get rid of this problem, the Underwater Friction Stir Welding (UWFSW) process can be employed. The water cooling reduces the heat, and thus, the desired thermal softening takes place in TMAZ and HAZ. Therefore, the material flow is entirely different in FSW and UWFSW. Since the weld defects, microstructural evolution, and mechanical properties are closely related to the material flow behavior during welding so it is important to control the material flow and heat distribution during joining.

UWFSW has been demonstrated to be a promising method for strength improvement of normal FSW joints. However, when improper welding parameters are used then welding defects, such as voids can be produced in the joints, leading to dramatically deteriorated mechanical properties. Thus to obtain high quality underwater joints, it is necessary to understand the variables that promote the formation of these defects. So, to overcome these defects appropriate and optimum parameters are required. The major significance of underwater FSW is in the field of lightweight alloys such as Aluminum alloys and Magnesium alloys. However, its application to metals such as steel, nickel and titanium has been also increasing.

Keywords: Alloy segregation; Solidification-related problems; TMAZ and HAZ; Friction stir welding

Introduction

The Friction Stir Welding (FSW) process was invented in 1991 by The Welding Institute (TWI) at Cambridge, United Kingdom. It was further developed and was got patented by the welding institute. The first built and commercially available friction stir welding machines were produced by ESAB welding and cutting products at their equipment manufacturing plant in Laxa, Sweden. The development of this process was a significant change from the conventional rotary motion and linear reciprocating friction welding processes. It provided a great deal of flexibility within the friction welding process group [1].

In 1991, in a flash of inspiration, Wayne Thomas realized that with the use of a rotational probe of a harder material than the workpieces, the workpiece material could be plasticized and an effective transportation mechanism could be provided for the plasticized material to join the workpieces together. This eventual moment of realization, after a long period of gestation, marked the discovery of FSW as we know it nowadays. Based on this discovery, the engineering restriction is quite low for applying the simple friction stir action provided by the probe for welding to a very large range of structures/parts and a wide range of weld geometry [2].

In 1993, NASA challenged Lockheed Martin Laboratories in Baltimore, Maryland, to develop a high strength, low-density, lighter weight replacement for aluminum alloy Al 2219 used on the original Space Shuttle External Tank. Lockheed Martin, Reynolds aluminum, and the labs at Marshall Space Flight Center in Huntsville, Alabama, were successful in developing a new alloy known as Aluminum Lithium (Al-Li 2195), which reduced the weight of the External Tank by 7,500 pounds (3,402 kilograms). Today, the external tank project uses the new alloy to build the Shuttle's super lightweight tanks. In 1997 the institute of materials research of the German aerospace center (DLR), was the first non-industrial research institute in Germany working in the field of friction stir welding of aluminum alloys and one of the first TWI licensees in Germany [3-6].

The basic concept of FSW is remarkably simple. A non-consumable rotating tool with a specially designed pin and shoulder is inserted into the abutting edges of sheets or plates to be joined and subsequently traversed along the joint line. Figure 1 illustrates process definitions for the tool and workpiece. Most definitions are self-explanatory, but advancing and retreating side definitions require a brief explanation. Advancing and retreating side orientations require knowledge of the tool rotation and travel directions. In Figure 1, the FSW tool rotates in the counterclockwise direction and travels into the page (or left to right). In Figure 1 the advancing side is on the right, where the tool rotation direction is the same as the tool travel direction (opposite the direction of metal flow), and the retreating side is on the left, where the tool rotation is opposite the tool travel direction (parallel to the direction of metal flow). FSW being a solid-state process eliminates many of the defects associated with fusion welding techniques such as shrinkage, solidification cracking, and porosity.
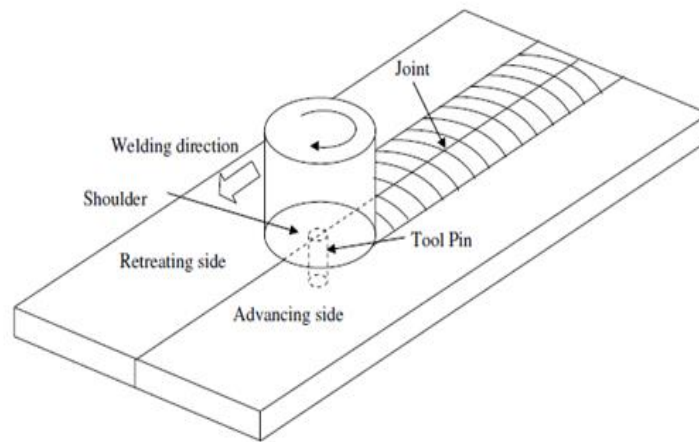

FIG.1. **Schematic drawing of Friction stir welding process.**

Friction stir welding was originally invented for welding aluminum, as some grades of aluminum are considered difficult to weld by existing arc welding techniques, and a few, such as the very high strength 2XXX and 7XXX series of alloys, are unwieldable.

A significant problem arises from the volatility of many of the alloying elements used to strengthen the aluminum: elements such as lithium are easily oxidized or even burned off during fusion welding and thus upon solidification the weld zone is no longer the same grade of material as the parent.

Aluminum and its alloys also undergo significant volume changes (up to 4%) during the melting and resolidification processes. This can cause very significant distortion of the components being welded, and give rise to solidification cracking due to the stresses involved. Friction stir welding, being a solid-state, mechanical process, does not encounter these problems to the same degree and can produce sound, low-distortion welds in all aluminum alloys, wrought and cast [7-10].

Since invented Friction Stir Welding (FSW) in 1991, TWI has continued to develop its potential. The technique continues to be advanced and refined for the joining of various materials such as aluminum, magnesium, copper and copper alloys, hafnium and zirconium, Inconel and super alloys, steel and ferrous alloys, titanium, dissimilar materials, and thermoplastics.

Work done to date

Though a lot of work has been done on the FSW the innovation on UWFSW is still in a nascent state and scarce work has been done to date. So, there are tremendous opportunities to explore the potential of UWFSW.

Sakurada were the first who used submersion in a rotary friction weld for 6061 aluminum alloys. Benavides performed an FSW experiment of 2024 aluminum alloy using liquid nitrogen to decrease the initial temperature of the samples from -30°C to 30°C. It was found that the hardness of the TMAZ and HAZ was remarkably improved, demonstrating the positive effect of external liquid cooling on joint performances. Fratini considered in-process heat treatment with water flowing on the top surfaces of welding samples during FSW and the tensile strength of the joint was improved to some extent. Hofmann reported that solid stirred zones in 6061 Al with fine grain sizes even less than 0.2 μm could be made by using Submerged Friction Stir Processing (SFSP) performed underwater. CLARK studied the underwater friction stir welding of 304 L stainless steel and the results revealed that the joints had better mechanical properties and were less susceptible to corrosion than the arc welding counterparts. Recently, LIU studied the underwater friction stir welding of 2219 aluminum alloy. The results showed that underwater FSW is available for the strength improvement of normal FSW joints and the welding parameters have an effect on the joint performance. Gaafer pointed out that the excess heat input induced by HRS could increase the fluidity of the metal and create turbulent flow at the weld zone, which may contribute to the formation of cavities; however, further investigation was not conducted to conclusively prove this point. Zhang reported that the performance of UWFSW joints of AA2219 Al alloy was enhanced by narrowing the width of the HAZ. Bloodworth adopted SFSW to improve the strength of the FSW joint of AA6061. Hofmann and Kenneth used submerged friction-stir processing as an improved method for creating ultrafine-grained bulk materials [10-12].

It is an advanced technique of welding. Few researchers have used the optimization technique in the field of friction stir welding but very little in the case of UFSW. UFSW is not fully explored yet.

Advantages of FSW

The process advantages result from the fact that the FSW process takes place in the solid phase below the melting point of the materials to be joined. The benefits include the ability to join materials that are difficult to fusion weld, for example, 2XXX and 7XXX aluminum alloys, magnesium and copper. Friction stir welding can use purpose designed equipment or modified existing machine tool technology. The process is also suitable for automation and is adaptable for robot use.

Other advantages are as follows:

- Low distortion and shrinkage, even in long welds
- Excellent mechanical properties in fatigue, tensile and bend tests
- No arc or fumes
- No porosity
- No spatter
- Can operate in all positions
- Energy efficient
- One tool can typically be used for up to 1000 m of weld length in 6XXX series aluminum alloys
- No filler wire required
- No gas shielding for welding aluminum
- Some tolerance to imperfect weld preparations - thin oxide layers can be accepted
- No grinding, brushing, or pickling is required in mass production
- Can weld aluminum and copper of >75mm thickness in one pass.

Why underwater

Studies on FSW of AA2519 aluminum alloy were made by Fonda and the study concluded that the TMAZ region exhibited the lower hardness and the tensile fracture also occurred in the TMAZ region. Liu reported that the TMAZ was the weakest zone in the friction stir welded AA2219 aluminum alloy joint and the tensile fracture exactly occurred in the LHDR. From the above references, it is understood that the hardness improvement in the joint is essential to improve the tensile strength of the joint. Post Weld Heat Treatment (PWHT) was employed to recover the hardness in the softer region by re-precipitation. However, the difference in grain size and dislocation densities in the various regions may result in heterogeneous precipitation during the aging

process. So, there exists a large gap between the parent metal properties and the joint properties. Instead of a secondary heat treatment process, the in-process water cooling during FSW is possible to yield better joint properties.

This process is termed as Underwater Friction Stir Welding (UWFSW) process. The water-cooling method is the easiest way to enhance the joint strength by FSW (Table 1) [13-16].

Advantages of underwater FSW:

TABLE.1. **Benefits of UWFSW.**

Metallurgical Benefits	Environmental Benefits	Energy Benefits
• Solid-phase process • Low distortion • Good dimensional stability and repeatability • No loss of alloying elements • Excellent mechanical properties in the joint area • Fine recrystallized microstructure • Absence of solidification cracking • Replace multiple parts joined by fasteners • Weld all aluminum alloys • Post-FSW formability	• No shielding gas required • Minimal surface cleaning required • Eliminate grinding wastes • Eliminate solvents required for degreasing • Consumable materials saving, such as rugs, wire, or any other gases • No harmful emissions	• Improved materials use (e.g., joining different thicknesses) allows a reduction in weight • Only 2.5% of the energy needed for a laser weld • Decreased fuel consumption in lightweight aircraft, automotive, and ship applications

Literature Review

Behavior of Aluminum in UWFSW

There is a tremendous change in the mechanical properties of aluminum in underwater friction stir welding, which is attributed to a change in grain size. The water also affects the heat dissipation behavior of weld and promotes superior properties to FSW in air. Some behavior change is given below:

Tensile strength: External liquid cooling leads to strength improvement due to improved grain structure and quick heat dissipation. The tensile strength firstly increases with increasing the welding speed from 50 to 150 mm/min and then dramatically decreases to a considerably low level owing to the formation of groove defect.

Grain size: The grain size evolves significantly with rotation speed. Much finer grains are observed at a lower rotation speed. As the rotation speed increases, the equiaxed grains grow remarkably due to the increase in heat input. Higher magnification micrographs of the stir zones give two other important observations. First, the dislocation density within the grains gradually increases with an increase in rotation speed, which should be attributed to the increase in deformation rate. Second, the precipitate evolution presents a similar feature in the SZ independent of rotation speed: nearly all the meta-stable precipitates have been dissolved into the matrix and only a few block shaped equilibrium precipitates with little strengthening effect on the matrix are observed in the grains. This implies that the temperature in the SZ is still high enough to dissolve the strengthening precipitates although external water cooling is applied during the welding [16-20].

Hardness: Increasing the rotation speed widens the softening region of the underwater joints; the maximum detrimental effect of thermal cycles on joint properties is weakened from 600 to 800 rpm and reaches a plateau in the rotation speed range of 800-1200 rpm. The occurrence of the plateau is attributed to the severe heat absorption capacity of water that can effectively control the temperature level of the weakest location of the joints. Nevertheless, if the rotation speed increases up to a rather high value (e.g., 1400 rpm), the heat input plays the dominant role and lowers the hardness minimum markedly [8].

Fracture: The fracture is occurring in the weakest region, *i.e.* at TMAZ. The FSW joints exhibit wider TMAZ, and the UWFSW joints exhibit narrow TMAZ near the weld periphery. Because of wider TMAZ, the fracture path is 45° to the loading direction and the failure is occurred by simple shearing. But in UWFSW joints, due to narrowed TMAZ, the fracture path is restricted near to the weld periphery, and thus, the shape of the fracture path is similar to the shape of the weld periphery. In addition, the grain orientation difference at the interface offers resistance to the tensile fracture, and thus, the fracture surface is not smooth [4].
Ductility: The weld joint underwent a reduction in the ductility property. The measures of ductility, *i.e.* elongation of the joints were lower than the parent metal.

The poor precipitation strengthening and grain boundary strengthening of TMAZ offers less resistance to tensile load. Therefore, the load was accommodated in TMAZ which cause the yielding of TMAZ. The load concentration phenomenon is called strain localization. Because of strain localization, the TMAZ alone contributes to elongation during tensile loading. Therefore, a reduced elongation value was observed in the joints compared to the parent metal. The elongation of joints is almost similar; however, the UWFSW joints exhibit lower elongation than the FSW joints. This was attributed to the narrow TMAZ of UWFSW joints which undergone high extent of strain localization than the FSW joints [4].

Material flow

The material flow patterns are utilized to explain the formation mechanisms of welding defects. (Figure 2a) shows the cross-section of a typical underwater joint, which was produced at a rotation speed of 1000 rpm and a welding speed of 200 mm/min. (Figure 2b–d) shows the microstructures of deformed zones of the joint. The material directly stirred by the welding tool is extruded around the RS and fills the hole at the rear of the tool. This part of the material undergoes intense plastic deformation and forms a region composed of fine recrystallized grains, which is commonly referred to as the SZ (Stir Zone).

The upper part of SZ mainly experiences the stirring action of the tool shoulder, while the lower part of SZ mainly experiences the stirring action of the tool pin; hence, the SZ displays different fine grain structures between its upper and lower regions (Figure 2c, d). In this article, the upper region of SZ is referred to as the Shoulder Stirred Zone (SSZ), and the lower region is referred to as the Pin Stirred Zone (PSZ).

The surrounding material constraining the SZ is deformed by the passage of the tool and forms the TMAZ. Therefore, the deformed zones of the underwater joint are composed of three parts, *i.e.* SSZ, PSZ, and TMAZ. For each deformed zone, especially the SSZ and TMAZ, the flow direction of the elongated base material grains are a reflection of the material flow direction. The material flow patterns of the deformed zones can be deduced from (Figure 2e) and are listed below.

- A part of the SSZ material transferred from the RS (Retreating Side) to the AS (Ascending Side) flows into PSZ along the long axis direction of the grains of the TMAZ. In the statements below, this flow pattern is defined as ''extruding reflux of SSZ material''. Due to different microstructures and flow directions, the material that undergoes extruding reflux shows clear boundaries toward TMAZ material and the remaining SSZ material. The extent of extruding reflux is determined by the amount of the SSZ material flowing back to AS and the interaction between SSZ material and TMAZ material.
- PSZ shows a typical ''onion ring'' structure except for the part adjacent to SSZ, where the onion rings become ambiguous, indicating a turbulent flow pattern.
- During FSW, a certain amount of TMAZ material is dragged into the pin hole under the effect of the rotating tool. Here, the quantity of TMAZ material is determined by the area of TMAZ grains within the pin profile [5].
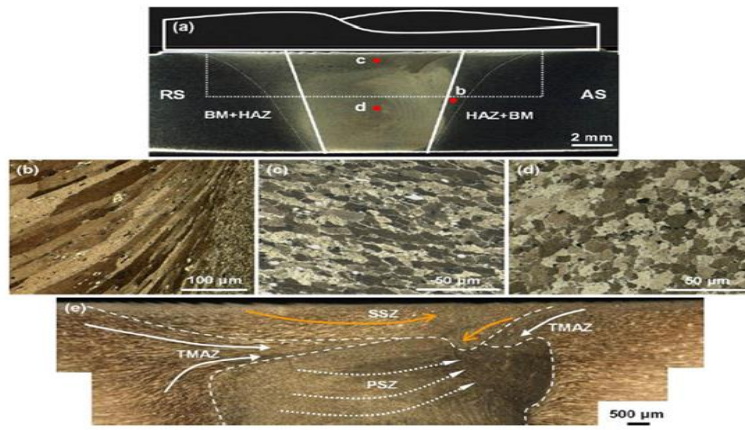
FIG.2. **Cross-section and microstructures of the deformed zones of a typical underwater joint. (a) Cross-section (b) TMAZ, (c) SSZ, (d) PSZ, (e) enlarged view of the microstructures in the dashed square of Figure 2a.**

Based on the material flow patterns in different zones of the joints, a material flow model of FSW is proposed, as shown in (Figure 3). During the welding process, the upper region of the pin-sheared material tends to be extruded into the concave area of the shoulder. This material, together with the shoulder-sheared material, flows around the RS with the shoulder and fills the hole at the rear of the welding tool, resulting in the formation of SSZ. The pin-sheared material that is not extruded into the concave part of the shoulder flows around the pin and fills the remaining hole behind the tool, which produces the PSZ. Despite the existence of tool tilt, the shoulder still rotates in a nearly horizontal direction during FSW. The height of the SSZ material that flows horizontally reflects the stirring effect of the shoulder on the workpiece in the thickness direction (*i.e.* the level of shoulder-driven flow). This height is defined as h_1. In the PSZ, the material experiences two flow patterns. One is the circle flow around the tool pin, and the other is the upward flow due to the shearing of pin threads. The minimum height of the PSZ adjacent to SSZ, defined as h_2, reflects the effect of pin-driven flow on the filling of the pinhole.
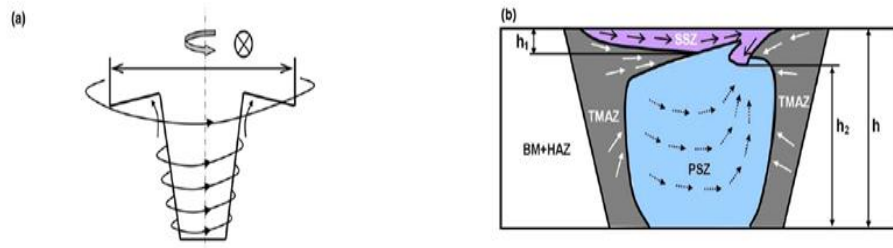

FIG.3. **Material plastic flow model for the underwater FSW; A Movement of the plastic material during FSW, b material flow patterns in the deformed zones of the joint.**

Many research works [15] was previously carried out to understand the flow behavior of materials in the FSW process, but limited research works have been reported so far related to the material flow behavior of UWFSW process (Table 2).

Parameters affecting the material flow

TABLE 2. **Parameters affecting the material flow**.

Tool design variables	Machine variables	Other variables
Shoulder and pin materials	Welding speed	Anvil material
Shoulder diameter	Spindle speed	Anvil size
Pin diameter	Plunge force or	Workpiece size

Pin length	depth	Workpiece
Thread pitch	Tool tilt angle	properties
Feature geometry		

Influence of rotation speed: As the rotation speed increases, h_1 is significantly increased but h_2 is gradually decreased. This suggests an improvement in the stirring effect of the shoulder and an enhancement of the upward flow of pin-sheared material. Additionally, the extruding reflux of SSZ material is increased on the AS with an increase in the rotation speed. When the rotation speed is increased up to 1400 rpm, turbulent material flow occurs in the PSZ adjacent to SSZ, and a void defect is observed at this location. With increasing the rotation speed, h_2 gradually decreases, but in contrast, slight variations occur in h_1. Furthermore, the amount of TMAZ material dragged into the pinhole increases with increasing rotation speed. At 1200 and 1400 rpm, the SSZ material flows into the pinhole in a downward direction, and welding defects such as voids and grooves are present in the joints. Before the occurrence of groove defect, the extruding reflux of SSZ material increases with increasing rotation speed [5].

Accordingly, the rotation speed must be chosen in a proper range to produce high-quality joints through underwater FSW. The present investigation demonstrates that too low or too high rotation speed can both yield poor joint properties. The former is owing to the inadequate tool stirring while the latter is attributed to the excess heat input. Therefore, the proper rotation speed should be chosen in such a way that the strain hardening induced by tool stirring can effectively improve the mechanical properties of the SZ whereas the heat input will neither seriously deteriorate the mechanical properties of the TMAZ and HAZ nor cause welding defects in the SZ.

Figure 4 shows cross-sectional micrographs and corresponding flow patterns for welds with a constant welding speed of 100 mm/min and different rotation speeds. As the rotation speed increases, h_1 is significantly increased but h_2 is gradually decreased (Figure 4a,c,e). This suggests an improvement in the stirring effect of the shoulder and an enhancement of the upward flow of pin-sheared material.

Additionally, the extruding reflux of SSZ material is increased on the AS with an increase in the rotation speed (Figure 4b,d,f). When the rotation speed is increased up to 1400 rpm, turbulent material flow occurs in the PSZ adjacent to SSZ, and a void defect is observed at this location. Weld cross-sections and corresponding material flow patterns for the conditions of a relatively high constant weld speed of 200 mm/min and varying rotation speeds are shown in (Figure 5). With increasing the rotation speed, h_2 gradually decreases, but in contrast, slight variations occur in h_1 (Figure 5a,c,e). Furthermore, the amount of TMAZ material dragged into the pinhole increases with increasing rotation speed. At 1200 and 1400 rpm, the SSZ material flows into the pinhole in a downward direction, and welding defects such as voids and grooves are present in the joints.

Before the occurrence of groove defect, the extruding reflux of SSZ material increases with increasing rotation speed (Figure 5b,d) [5].
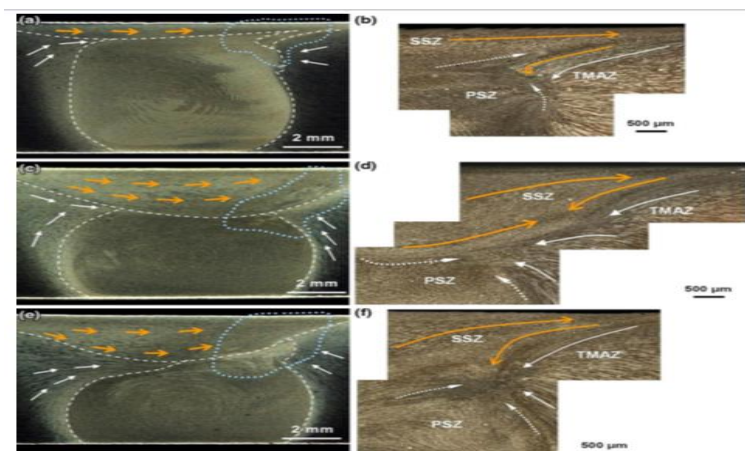

FIG.4. **Cross sections and material flow patterns of the joints obtained at different rotation speeds and a constant welding speed of 100 mm/min. a, c, and e Cross sections obtained at 1000, 1200, and 1400 rpm, respectively; b, d, and f material flow patterns corresponding to (a), (c), and (e).**
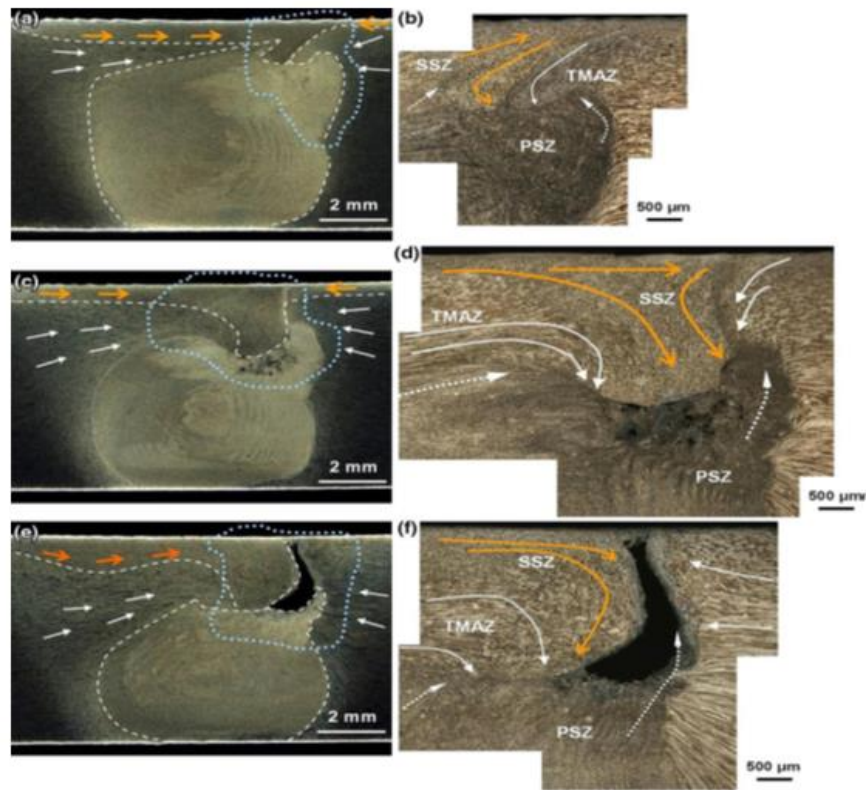
FIG.5. **Cross sections and material flow patterns of the joints obtained at different rotation speeds and a constant welding speed of 200 mm/min. a, c, and e Cross sections obtained at 1000, 1200, and 1400 rpm, respectively; b, d, and f material flow patterns corresponding to (a), (c), and (e).**

Influence of welding speed: With increasing weld speed, h_1 and h_2 exhibit little variation from 100 to 200 mm/min but decrease at 300 mm/min. This implies that increasing the welding speed not only weakens the stirring effect of the shoulder but also enhances the upward flow of pin-sheared material. Extruding reflux of SSZ material occurs at 100 mm/min. At 200 mm/min, this phenomenon becomes more severe, leading to the turbulent flow in the PSZ; simultaneously, a certain quantity of TMAZ material is dragged into the pinhole. At the higher rotation speed of 300 mm/min, more TMAZ material is involved in the filling process of the pinhole. When this part of TMAZ material stops flowing, SSZ material then flows into the pinhole in a downward direction, and in this case, avoid defect is observed in the joint h_1 is greatly decreased when the rotation speed increases from 100 mm/min to the range of 200–250 mm/min; additionally, h_2 also decreases progressively with increasing welding speed. At 200 mm/min, a large amount of TMAZ material is involved in filling the pinhole. The SSZ material flows into the pinhole in a downward direction, and a void defect is formed at the PSZ adjacent to SSZ. At a higher welding speed of 250 mm/min, more TMAZ material is dragged into the pinhole, and the SSZ material exhibits a greater tendency for downward flow. A groove defect is formed in the joint under these conditions.

Figure 6 shows the cross-sections and material flow patterns of welds produced at different welding speeds and a constant rotation speed of 1000 rpm. With increasing weld speed, h_1 and h_2 exhibit little variation from 100 to 200 mm/min but decrease at 300 mm/min (Figure 6a,c,e). This implies that increasing the welding speed not only weakens the stirring effect of the shoulder but also enhances the upward flow of pin-sheared material. Extruding reflux of SSZ material occurs at 100 mm/min. At 200 mm/min, this phenomenon becomes more severe, leading to the turbulent flow in the PSZ; simultaneously, a certain quantity of TMAZ material is dragged into the pinhole (Figure 6c,d). At the higher rotation speed of 300 mm/min, more TMAZ material is involved in the filling process of the pinhole.

When this part of TMAZ material stops flowing, SSZ material then flows into the pinhole in a downward direction, and in this case, a void defect is observed in the joint (Figure 6e,f).

Figure 7 shows cross-sections and material flow patterns of the welds produced at different welding speeds and a constant rotation speed of 1200 rpm; h_1 is greatly decreased when the rotation speed increases from 100 mm/min to the range of 200–250 mm/min; additionally, h_2 also decreases progressively with increasing welding speed Figure 7a,c,e. At 200 mm/min, a large amount of TMAZ material is involved in filling the pinhole (Figure 7c).

Similar to the observations for Figure 6f, the SSZ material flows into the pinhole in a downward direction, and a void defect is formed at the PSZ adjacent to SSZ (Figure 7d). At a higher welding speed of 250 mm/min, more TMAZ material is dragged into the pinhole, and the SSZ material exhibits a greater tendency for downward flow (Figure 7e, f). A groove defect is formed in the joint under these conditions.
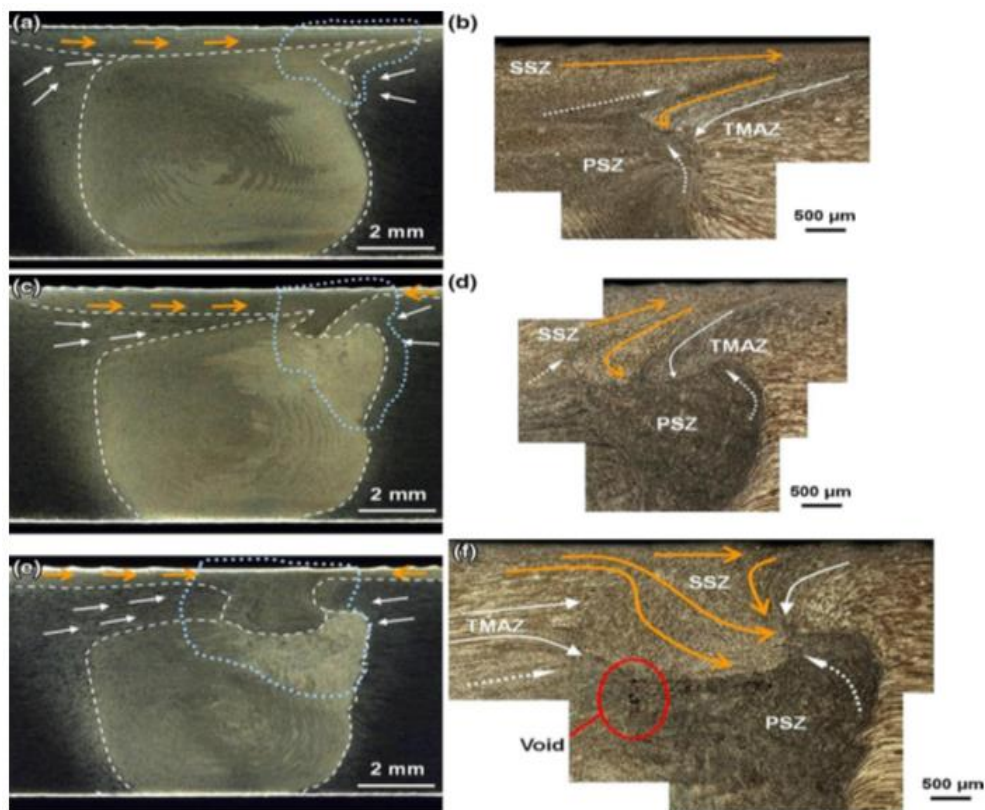

FIG.6. **Cross sections and material flow patterns of the joints obtained at different welding speeds and a constant rotation speed of 1000 rpm. a, c, and e Cross sections obtained at 100, 200, and 300 mm/min, respectively; b, d, and f material flow patterns corresponding to (a), (c) and (e).**
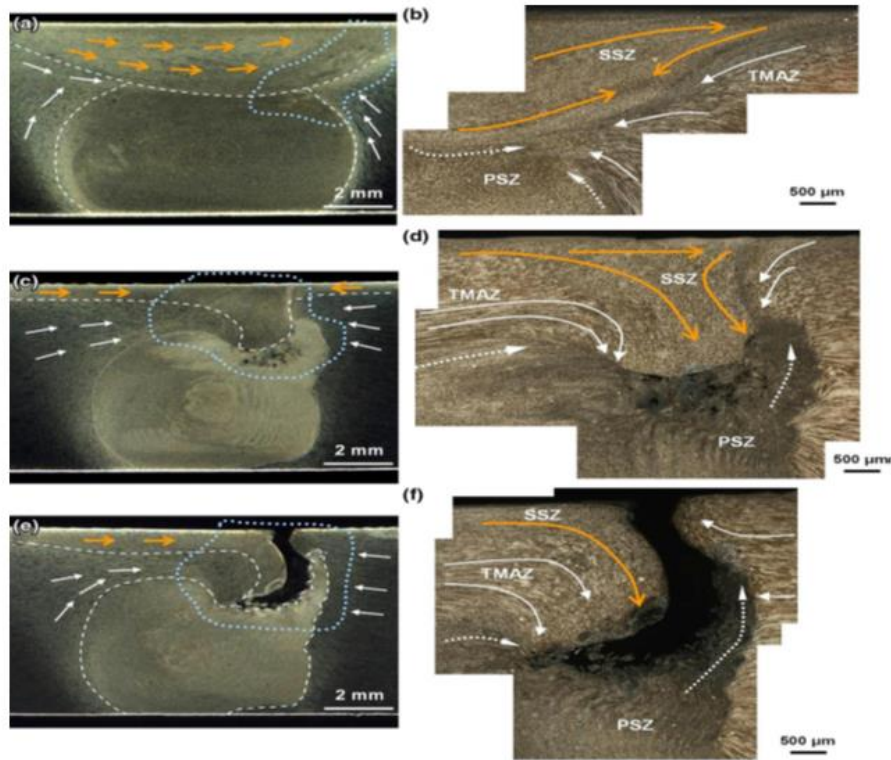
FIG.7. **Cross sections and material flow patterns of the joints obtained at different welding speeds and d constant rotation speed of 1200 rpm. a, c and e Cross sections obtained at 100, 200, and 250 mm/min, respectively; b, d, and f material flow patterns corresponding to (a), (c) and (e).**

Tool tilt and plunge length: The plunge depth is defined as the depth of the lowest point of the shoulder below the surface of the welded plate and is a critical parameter for ensuring weld quality. Plunging the shoulder below the plate surface increases the pressure below the tool and helps ensure adequate forging of the material at the rear of the tool. Tilting the tool by 2-4 degrees, such that the rear of the tool is lower than the front, has been found to assist this forging process.

Given the high loads required the welding machine may deflect and so reduce the plunge depth compared to the nominal setting, which may result in flaws in the weld. On the other hand, an excessive plunge depth may result in the pin rubbing on the backing plate surface or a Significant under match of the weld thickness compared to the base material. Variable load welders have been developed to automatically compensate for changes in the tool displacement while The Welding Institute (TWI) has demonstrated a roller system that maintains the tool position above the weld plate [3].

Shoulder diameter: The shoulder diameter must be not too large to minimize the width of the welding zone line. In other words, if the shoulder diameter is too large, it will cause a wide section of the plate to be plasticized. The shoulder diameter is usually taken as double the pin diameter. Experimental investigations have shown that only a tool with an optimal shoulder diameter result in the highest strength [3].

Shoulder surface and geometry: The nature of the tool shoulder surface is an important aspect of tool design. Flat, convex and concave tool shoulders and cylindrical, tapered, inverse tapered and triangular pin geometries are used. They found that triangular pins with concave shoulders resulted in high-strength spot welds. The microstructure, geometry, and failure mode of a weld may be significantly altered if the tool shoulder chosen is concave rather than flat. The FSW process with convex scroll shoulder tends to be stable with a nearly constant plunge depth. The conventional rotating shoulder tools can result in high thermal gradients and high surface temperatures during FSW of low thermal conductivity alloys leading to the deterioration of weld quality. A stationary shoulder friction stir welding process has been developed by The Welding Institute in which the non-rotating shoulder slides on the workpiece surface as the rotating pin moves forward (Figure 8,9,10) [3].
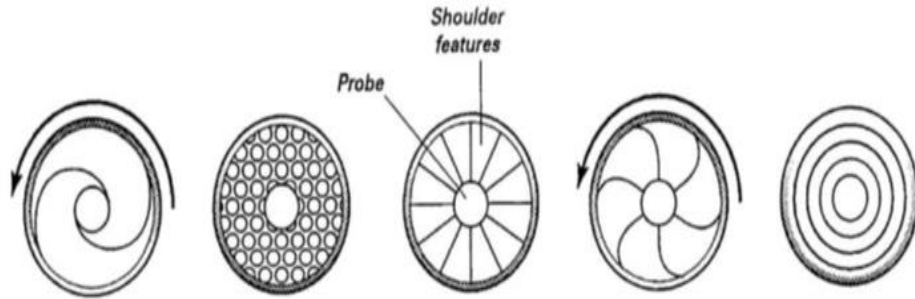
FIG.8. **Different shoulder features used to improve material flow and shoulder efficiency.**

Pin geometry: The shape of the tool pin (or probe) influences the flow of plasticized material and affects weld properties. A triangular or 'trifluted' tool pin increases the material flow compared with a cylindrical pin. The axial force on the workpiece material and the flow of material near the tool are affected by the orientation of threads on the pin surface. Features such as threads and flutes on the pin are believed to increase heat generation rate due to larger interfacial area, improve material flow and affect the axial and transverse forces [3].
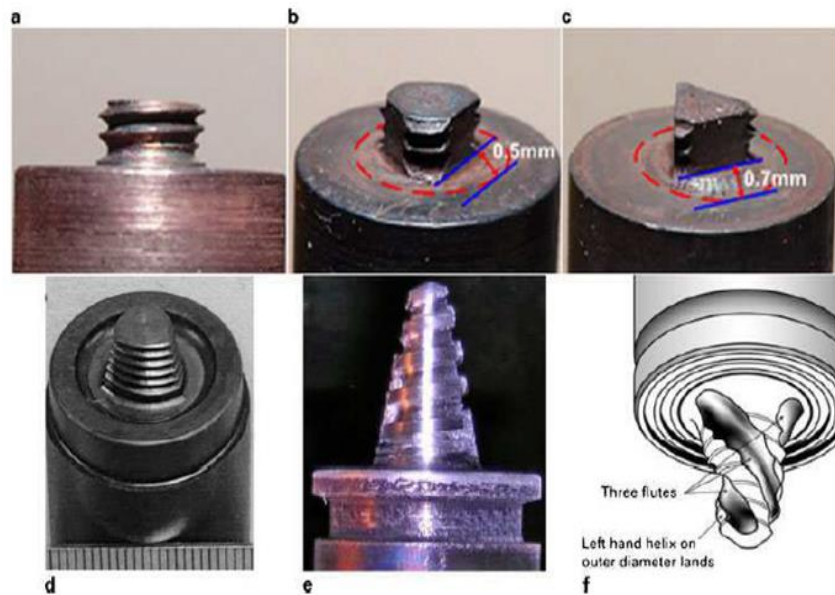

FIG.9.**Commonly used tool pin geometries-(a)cylindrical threaded;(b)three flat threaded;(c)triangular;(d)trivex; (e)threaded conical; (f)schematic of a triflute.**

Anvil size or material: The anvil size and material can have a dramatic effect on process forces and heat generation in FSW, based on their role in thermally preconditioning the workpiece material in advance of the welding tool. This self-referential relationship contributes to the stability of the welding process, but at the same time, it complicates the determination of the effect of process variables on heat generation [3].

Welding tools: Tools consist of a shoulder and a pin which can be integral with the shoulder or as a separate insert possibly of a different material. The design of the shoulder and the pin is very important for the quality of the weld [3].

Tool materials: Welding tool material development has enabled the welding of high melting point materials, such as titanium, steel and copper, and has improved productivity in aluminum welding. Tool steel materials are generally acceptable for the FSW of aluminum alloys. However, much like the situation today with welding tool geometry, even for welding aluminum alloys there is no accepted standard tool material. For applications where aluminum alloys from 6 to 12 mm thickness are welded, H-13 tool steel is generally adequate. For such applications, it is also often possible to use a one-piece welding tool design. However, if

high productivity is needed or it is necessary to weld thicker aluminum materials, a more elaborate tool design and material selection may be required. In such cases, the pin might be made from a material that has higher strength at the temperature of welding, such as MP-159, while the shoulder might still be made from H-13. For applications that require welding other materials, such as titanium, steel, and copper, welding tools might be made from tungsten-based materials, polycrystalline cubic boron nitride, or any number of other materials that offer high performance at high temperatures [3].

Tool geometry: Figure 6 shows the tools with four different pin profiles, namely Straight Cylindrical (STC), straight Threaded Cylindrical (THC), Taper Cylindrical (TAC), and taper Threaded Cylindrical (TTC). Tapering of the tools is a must. So, STC and THC tools that are not tapered produce tunnel defects. So, they are highly prohibited tools to use. Now, out of the other two tools, TTC shows superior and best joint properties. It is attributed to the attainment of a balanced state of heat generation and material flow during stirring. TTC joint exhibited higher tensile strength and joint efficiency than any other tool. The presence of relatively finer grains in the stir zone, the higher volume fraction of precipitates, marginally higher hardness of stir zone, and appreciably lower width of lower hardness distribution region are the main reasons for the better performance of TTC joints than its counterparts (Table 3).
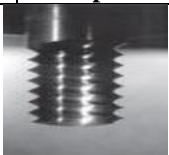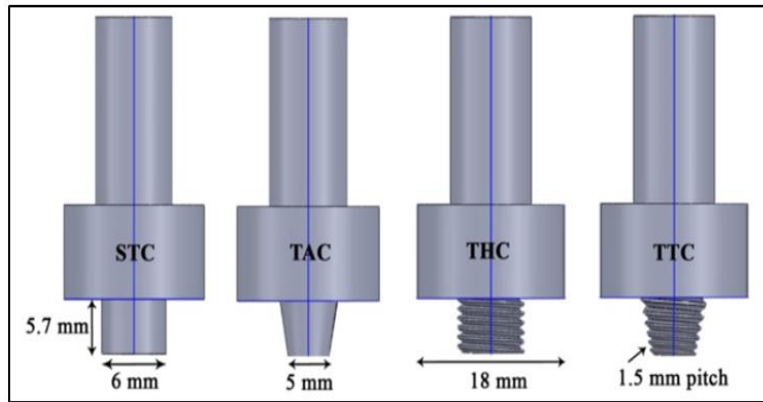

FIG.10. **Dimensions of the tool pin profiles.**

TABLE 3. **Various tool pin profiles.**

Feature	Intended effect	Examples
Threads on pin	Compression of the weld zone against anvil.	
Flats or other reentrant features	A new mode of plastic work, thicker section welding, higher heat input.	
Flat pin tip	Improved TMAZ penetration, higher penetration ligaments better robustness.	
Frustum pin profile	Reduced lateral forces, thicker section welding.	

Flare pin profile	Wider root profile.	
Shoulder scrolls	Elimination of tool tilt requirement, containment of softened workpiece material.	
Tapered shoulder	Variable shoulder contact width, variable shoulder penetration.	

Aluminum alloys

Aluminum-copper alloy

2219-T6 Aluminum Alloy: Heat-treatable aluminum alloys with favorable strength-to-weight ratios are widely used in aircraft and aerospace applications. Regarding the FSW of heat-treatable aluminum alloys, although the thermal flow does not cause any material fusion, it still exerts a thermal action on the material to be welded and deteriorates the local mechanical characteristics through the coarsening or dissolution of strengthening precipitates. In recent years, of particular interest is to improve the joint properties by controlling the temperature level. To do so, the liquid medium was commonly chosen to perform an in-process cooling on the welding samples during FSW. Fratini considered in-process heat treatment with water flowing on the top surfaces of welding samples during FSW and the tensile strength of the joint was improved to some extent. To take full advantage of the heat absorption capacity of water, an underwater FSW of 2219-T6 aluminum alloy was conducted, during which the whole workpiece was immersed in the water environment. The results indicated that the tensile strength of the underwater joint was higher than that of the normal joint, confirming the feasibility of underwater FSW to improve the joint properties. Although external liquid cooling has been demonstrated to be available for strength improvement in the previous studies, the relationship between the process variables and the performance of the cooled joints has not yet been developed (Tables 4 and 5).

TABLE 4. **Chemical compositions and mechanical properties of 2219 aluminum alloy.**

Chemical compositions (wt%)									Mechanical properties		
Al	Cu	Mn	Fe	Ti	V	Zn	Si	Zr	Tensile strength	Elongation	Hardness
Bal.	6.48	0.32	0.23	0.06	0.08	0.04	0.49	0.2	432MPa	11%	120-130 Hv

TABLE 5. **Tool size and welding parameters used in the experiments.**

Tool size (mm)				Welding parameters		
Shoulder diameter	Pin diameter	Pin length	Rotation speed (rpm)	Welding speed (mm/min)	Axial load (kN)	Tool tilt (∘)
22.5	7.5	7.4	600-1400	50-200	4.6	2.5

The Base Material (BM) used for the experiment was a 7.5 mm thick 2219-T6 aluminum alloy, whose chemical compositions and mechanical properties are listed in Table 4. The plate was machined into rectangular welding samples with dimensions of 300 mm long by 100 mm wide. After being cleaned with acetone, the samples were clamped to the backing plate in a vessel, and then the water at room temperature was poured into the vessel to immerse the top surface of the samples. Butt welds were made underwater using an FSW machine (FSW-3LM-003) along the longitudinal direction (perpendicular to the rolling direction) of

the welding samples at a fixed welding speed and various rotation speeds. Figure 11 shows the schematic view of the underwater FSW process. The welding tool consisted of a 22.5 mm/diameter shoulder and a conical right-hand screwed pin with a length of 7.4 mm and a median diameter of 7.4 mm. During the FSW, a 2.5º tilt and an axial load of 4.6 kN were applied to the welding tool. The welding speed was 50-200 mm/min and the rotation speeds were 600, 800, 1000, 1200, and 1400 rpm.
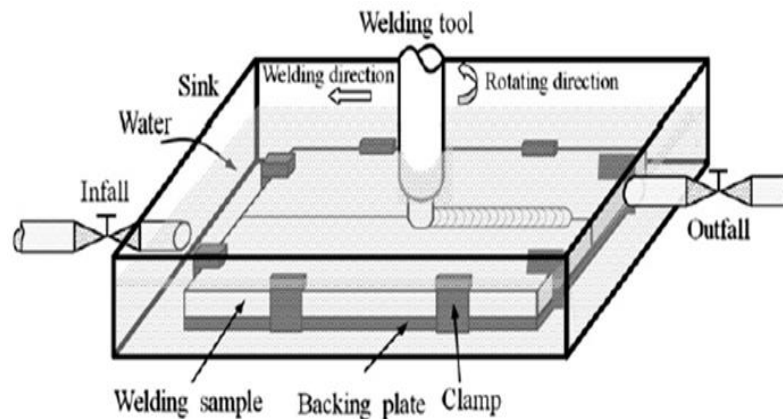

FIG.11.**The schematic view of underwater FSW.**

After welding, the joints were all cross-sectioned perpendicular to the welding direction for metallographic analyses and Vickers's hardness tests using an electrical-discharge cutting machine. The cross-sections of the metallographic specimens were polished using a diamond paste, etched with Keller's reagent and observed by Optical Microscopy (OM, Olympus-MPG3) [6]. Micro-hardness profiles were measured at the mid-thickness of the polished cross-sections with a spacing of 1 mm between the adjacent indentations. The testing load was 4.9 N for 10 s.

The transverse tensile specimens were cut perpendicular to the welding direction from the joints concerning China National Standard GB/T2651-2008 (equivalent to ASTM B557-02). The room temperature tensile test was performed at a crosshead speed of 1 mm/min using a computer-controlled testing machine (Instron-1186). The tensile properties of each joint were evaluated using three tensile specimens cut from the same joint. After the tensile test, the fracture features of the joints were analyzed by the OM mentioned above.

AA2519-T87 aluminum alloy: AA2519-T87 is a new armor-grade aluminum alloy employed in the fabrication of light combat military vehicles. Rolled plates of AA2519-T87 aluminum alloy were used as the parent material in this investigation (Table 6). The chemical composition of the parent metal was quantified using spectrochemical analysis and the composition is presented in Table. The joint configuration of 150 × 150 × 6 mm was used and the welding was done normally to the rolling direction using the tools with four different pin profiles, namely Straight Cylindrical (STC), straight Threaded Cylindrical (THC), Taper Cylindrical (TAC) and Taper Threaded Cylindrical (TTC).

TABLE 6. **Chemical composition of the alloy, Welding parameters and tool dimensions used in this investigation.**

Chemical composition (wt%)		Process parameters	Values
Cu	5.71	tool rotation speed (rpm)	1300
Mg	0.47	Welding speed (mm/min)	30
Mn	0.27	Pin Length (mm)	5.7
iFe	0.10	Tool shoulder diameter (mm)	18
V	0.05	Pin diameter (mm)	5-6
Si	0.04	Tool tilt angle (degree)	2
Ti	0.02	Pin profile	Taper threaded pin profile
Al	Balance	Tool material	Hardened super high steel

The joints were fabricated under air and water cooling mediums, and they are designated as FSW and UWFSW joints, respectively. The process parameters and the welding conditions used in FSW and UWFSW processes are presented in Table 5. These welding parameters were selected based on trial experiments to attain defect-free, sound joints. The specimens were extracted from the joints to test and characterize the FSW and UWFSW. Metallographic procedures were followed to reveal the microstructural characteristics of the welds by Optical Microscopy (OM). The OM specimens were polished using water emery papers and etched using Keller's reagent for 10 s to reveal the microstructure. The grain size of the stir zone is measured in the Pin-Influenced Region (PIR). Similarly, the grain size of TMAZ and HAZ is measured in the mid-thickness region.

One hundred kilos Newton servo-controlled universal testing machine (Make: FIE–BLUESTAR, India, Model: UNITEK 94100) was employed to evaluate the transverse tensile properties of the FSW and UWFSW joints. The tensile specimens were extracted, machined, and tested as per the ASTM E8M guidelines. Before testing, the samples were flattened to ensure an equal cross-sectional area along the entire gauge length of the specimen. The tensile properties such as yield strength, ultimate tensile strength, and elongation were evaluated. The cross-section of the tensile tested samples was polished and etched to reveal the entire fracture path using an optical microscope. The tensile fracture path was identified by the macro-structural analysis. A Scanning Electron Microscope (SEM) was employed to characterize the fracture surfaces. Hydraulic-controlled Vickers's micro-hardness tester (Make: Shimadzu and model: HMV-2T) was used to measure the micro-hardness along the cross-section of the weld joint. The indentations were made under the load of 4.9 N for a dwell time of 15 s. The single hardness profile was obtained along the mid-thickness region with the indentation of 1 mm spacing. The correlation between the entire fracture path and the LHDR cannot be agreed upon from the single hardness profile. Hence, the hardness distribution maps were obtained by indenting along five test lines which are 1 mm spacing along the thickness direction. In each test line, 25 indentations were made and a total of 125 indentations were made to obtain the hardness distribution map.

A Transmission Electron Microscope (TEM) was employed to characterize the microstructure of the LHDR (Low Hardness Distribution Region). A thin sample of 1mm thick was extracted from the weld joints using the Wire-cut Electro-Discharge Machining (WEDM) process. The samples were polished to 100 μm thick, and then a 3 mm diameter of the sample was extracted from the LHDR for further polishing. The samples were reduced to 10-μm thick using an ion milling process to reveal the microstructure under TEM.

2017 aluminum alloy (Ultrafine Grained): Ultrafine-Grained (UFG) materials (mean grain size $\leq$ 1μm) have some excellent physical and mechanical properties such as high strength, good toughness, and super-plasticity due to their unusual structure. UFG materials have been processed by Severe Plastic Deformation (SPD) techniques, such as torsion straining, Accumulative Roll Bonding (ARB), multiple forging and Equal Channel Angular Pressing (ECAP). Among all the SPD techniques, ECAP is especially attractive because it can introduce intense strains into samples without changing the cross-section area, thus large bulk materials with ultrafine grains can be produced by repeated deformation [7]. In many industrial applications, the joining of UFG materials is indispensable for building large constructions, which makes it a challenge to retain the fine microstructures and properties of UFG materials. FSW is found to be an attractive joining method for UFG aluminum alloys considering the significantly lower heat input than the fusion welding process. However, it is noticed that thermal cycles generated by the friction between the rotational tool and the workpieces will inevitably lead to a temperature rise in the joint, which may result in the coarsening of UFG materials during FSW. Therefore, the weld heat input control seems to be very important for welding performances. 2017 Al alloy plates with a UFG structure were prepared by ECAP, and then were friction stir welded underwater. The microstructural and mechanical characteristics of the underwater FSW joint were investigated.

The starting material was hot-rolled commercial 2017 Al alloy with the chemical composition given in Table. The average initial grain size was measured to be ~100 μm and the micro-hardness was approximately HV 81. The hot-rolled plates were treated at 350°C for 1 h and dry quenched to room temperature. Samples with dimensions of 14.5 mm × 14.5 mm × 80 mm for ECAP were cut from the plates [7]. The ECAP was performed up to four passes at room temperature using the solid die which had an intersection angle of 90° between the two channels and an outer curvature of 20°. Between consecutive passes, ECAP pressed samples were treated at 200°C for 30 minute and rotated by 90° in the same directions using route B_c (Table 7).

TABLE 7. **Chemical composition of 2017 aluminum alloy (mass fraction %).**

Cu	Mg	Mn	Fe	Si	Zn	Ni	Ti	Al
3.8-4.8	0.4-0.8	0.4-0.9	0.7	0.7	0.3	0.1	0.15	Bal.

The ECAP pressed specimens were cut into samples with dimensions of 3 mm × 14.5 mm × 80 mm [7] for the welding process. Underwater FSW was conducted on a retrofitted X5032 vertical milling machine. A non-consumable tool made of high-speed steel was used to fabricate the joints. The straight cylindrical pin was 3.6 mm in diameter and 2.8 mm long and the tool shoulder was 12 mm in diameter. The specimens were fixed to the bottom sheet in a rectangular tank which was secured on the milling table, and then circulating tap water was injected into the tank to immerse the top surface of the specimens. The rotating tool moved along the weld line, the employed rotational rate of the tool was 950 rpm and the travel speed was 60 mm/min.

After the welding process, metallographic samples were cross-sectioned perpendicular to the welding direction, mechanically polished, and then etched with Keller's reagent (190 mL water, 5 mL nitric acid, 2 mL hydrofluoric acid, and 3 mL hydrochloric acid) and analyzed by optical stereoscope (Nikon SMZ100) and Scanning Electron Microscope (SEM,S-3400N) equipped with Energy Dispersive Spectrum (EDS) analysis system. Transmission Electron Microscope (TEM) samples were extracted from the starting material, the as-pressed plates, and the FSW joint at mid-thickness. Thin foils for TEM investigation were ground to a thickness of ~50 μm and twin-jet electro-polished using a solution of 30% nitric acid-methanol at 30°C. TEM observations were carried out on a JEM-200CX instrument operating at 200 kV. Measurements of the grain size were made directly from the TEM images using the linear intercept method. The phase structure of the ECAP pressed material and the weld nugget zone was identified by the X-ray Diffraction (XRD) method on a Rigaku D/max 2400 instrument using Cu K_α radiation. Micro-hardness profile of the FSW joint was measured on the centerline of the cross-section perpendicular to the welding direction, using a 401 MVD micro-hardness tester with a load of 2 N for 10 s.

Aluminum-zinc alloy

7055-T6 aluminum alloy: Spray formed ultra-high strength aluminum alloy has been widely used in the aerospace and automotive industries due to its excellent properties, *i.e.* high strength, low density, and outstanding machinability. Its welding technology is also an advanced research hotspot. Friction Stir Welding (traditional FSW) is an accepted method for aluminum alloy welding. However, it still can't meet the welding requirement of spray-formed aluminum alloys.

Underwater Friction Stir Welding (UFSW) through modifying the thermal cycle of workpieces by water environment is successfully applied in many ultra-high-strength aluminum alloys welding as well as spray-formed aluminum alloy. The tensile properties, microstructure, corrosion resistance and the thermal cycle of underwater FSW joint had been compared with that of the traditional one. To optimize the properties of friction stir welded joints further, many studies target the adjustment of traditional FSW welding parameters. The UFSW process contains an interaction of the action of the pin tool and the cooling water which presents a unique feature that differs from traditional FSW. So when it discusses the adjustment of welding parameters, the cooperation with the water environment must be taken into account.

In the experiment, spray-formed 7055 aluminum (T-6) is used as the Base Metal (BM). The composition and the welding parameters are given in Table 7. The 4 × 250 × 100 mm sheets are prepared for the butt joint [9]. The FSW process was carried out by the FSW-3LM-002 machine produced by China Friction Stir Welding Center and the water-immersed environment is provided by a water tank as shown in Figure 12.

The thermal measurement system was added to monitor the change of temperature on the plate during the welding process and the position of thermocouples was shown in Figure 13 the RS is represented as retreaded side, and AS is represented as the advanced side of the weld. The water tank was full of water and test pieces were immersed in the water totally during the whole FSW process. The pin tool is made of H-13 steel consisting of a concave 10 mm diameter shoulder and a 4 mm diameter pin with a length of 3.75 mm.

During the FSW, a constant tile angle of 3° was maintained and the welding parameters were set as shown in Table 8. The parameter design in each group is settled by fold change in rotation speed (group S) or traveling speed (group F and F').
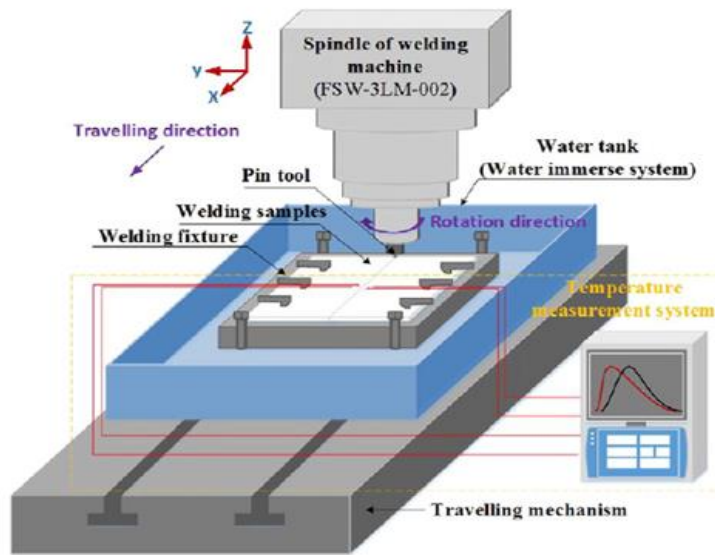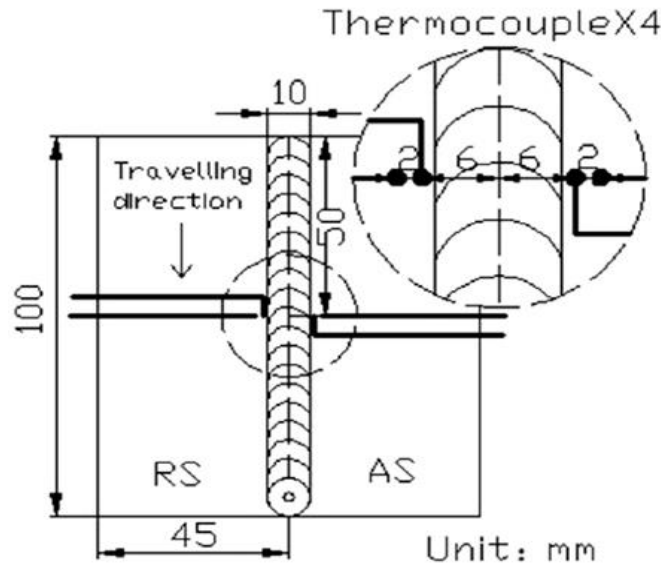
FIG.12. **Underwater FSW system.**

FIG.13. **The positions of thermocouples in the sample.**

TABLE 8. **Chemical composition of the alloy and the welding parameters for the experiments.**

Chemical composition %		Group	Number	Welding parameter		Remark
Al	Bal.			Traveling speed (mm/min)	Rotation speed (rpm)	
Cu	2.3	S	1		750	Fixed high traveling speed, different rotation speed
Mn	0.05		2	155	1050	
Cr	0.04		3		1550	
Fe	0.15		4		3000	
Si	0.1	F	1	155		

				105	750	Fixed low rotation speed, different traveling speed
Ti	0.06		2			
			3	75		
		F'	1	75		
			2	155	1550	Fixed high rotation speed, different traveling speed
			3	300		

After welding, tensile tests were carried out according to ASME BPVC section IX-2015. Metallographic specimens were cut from joint perpendicular to traveling direction and were with Keller's reagent (2 ml HF (48%)+3 ml HCl (37%)+5 ml HNO$_3$ (65%)+190 ml distilled water). Optical Microscopy (OM) was used for observing the macro profiles of joints. Scanning Electron Microscope and Energy Dispersive Spectrometer (SEM and EDS) was applied to observe the microstructure of the joints and X-ray Diffraction (XRD) was used in determining strengthening precipitates in joints [9].

UFSW of steels: The welding of steel enhances the vitality of FSW. Though FSW is accompanied by limitations because the thermal cycles applied to the FSW samples reduced the mechanical properties of the joints.

Although the low heat input generated during FSW does not lead to the melting of the base metal improving the strength of normal FSW joints by accelerating the heat dissipation.

This can be explained by considering the difference in heat input between each of the weld and FSW plates could be attributed to the fact that FSW plates are subjected to a higher degree of restraint during welding because of the clamping involved.

 This restraint mitigates movement during welding and hence reduces distortion. The SAW process involves a phase change during welding as it goes from liquid to solid, whereas FSW is a solid-state process.

This means that the magnitude of the thermal stresses will be larger for the Submerged Arc Welding (SAW) plate due to the volume changes (longitudinal and transverse shrinkage) experienced during solidification and subsequent cooling to room temperature. It is to be noted that Charpy impact toughness is significantly reduced for the underwater FSW, attributed ostensibly to a faster cooling rate due to the water environment while the strength, hardness, or fatigue life of the material increases.

UWFSW of dissimilar alloys

Aluminum-magnesium alloys: With the invention of FSW in 1991 a new scope for solid-solid welding has emerged showing a promising technique for welding dissimilar alloys like Al alloys and Mg alloys. This alloy has a significant application in a plethora of fields including shipbuilding, aerospace, automobile and railway.

On welding this alloy using FSW we encounter a cracking problem which is attributed to the lowering melting temperature of eutectic mixture leading to constitutional liquid and formation of inter-metallic like Al_3Mg_2 and $Al_{12}Mg_{17}$. So, we devised a new approach of submerged FSW in which the welding is done under liquid nitrogen which helps in lowering peak temperature and helps in controlling the inter-metallic formation and helps in getting finer microstructure attributed to dynamic recrystallization (Tables 9 and 10).
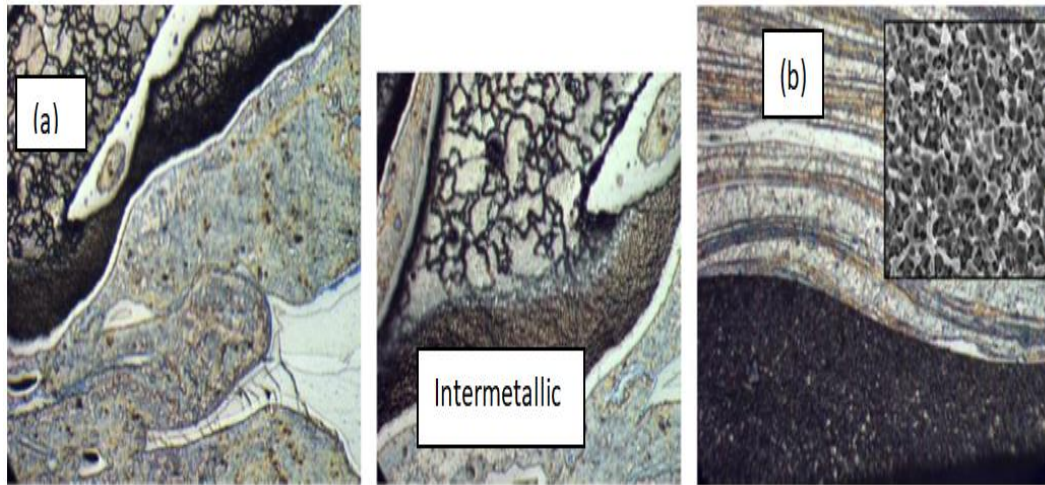
FIG. 14. **Microstructure of Al/Mg interface for friction stir welded specimen performed in (a) air (b) liquid nitrogen.**

Results

2219-T6 Aluminum alloy

TABLE 9. **Chemical compositions and mechanical properties of 2219 aluminum alloy.**

Chemical compositions (wt%)									Mechanical properties		
Al	Cu	Mn	Fe	Ti	V	Zn	Si	Zr	Tensile strength	Elongation	Hardness
Bal.	6.48	0.32	0.23	0.06	0.08	0.04	0.49	0.2	432 MPa	11%	120-130 Hv

TABLE 10. **Tool size and welding parameters used in the experiments.**

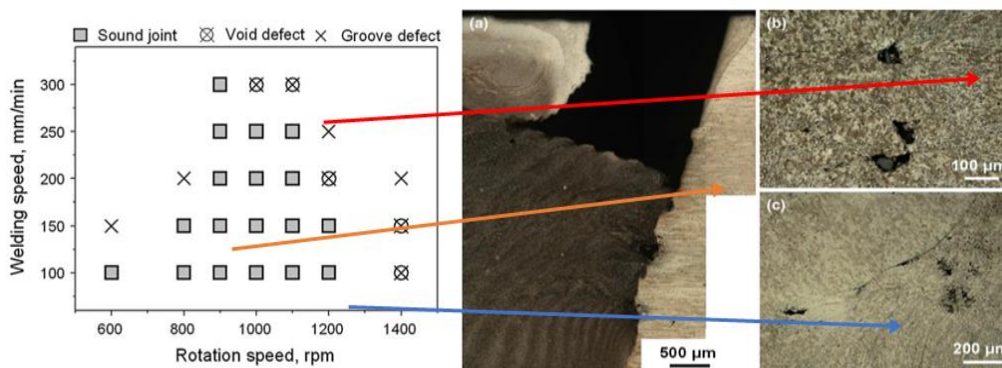| Tool size (mm)			Welding parameters			
Shoulder diameter	Pin diameter	Pin length	Rotation speed (rpm)	Welding speed (mm/min)	Axial loa (kN)	Tool tilt (°)
22.5	7.5	7.4	600-1400	50-200	4.6	2.5

FIG.15. **Influence of process parameters on the quality of underwater joints.**

During both normal and external liquid cooling FSW if any improper or inconsistent parameters like welding speed, rotation speed tool geometry, tilt angle, etc. are chosen then it led to several welding defects such as void, groove, tunnel, etc. at the weld

joint which can drastically deteriorate the mechanical properties. So it is very critical to analyze and characterized the welding defects [5-8].

The study of previous defects in normal FSW can be used to reveal the defect form in UFSW. Our core concern is on two aspects, one is to analyze the characteristics of defects formed in external liquid cooling FSW so that it can be used to provide a smooth path for process optimization in the future. The second aspect is the classification of the formation mechanism of weld defects produced at a high rotation speed [5-8].

Figure 14 shows how the weld quality evolves with varying rotation speed and welding speed. It is clear from the figure that Low Rotation Speed (LRS) and High Rotation Speed (HRS) both can lead to welding defects. In the LRS range of 600-800 generally, groove defect is formed at the Stir Zone (SZ) and the Thermo-Mechanical Affected Zone (TMAZ) interface on the AS due to insufficient heat input. If the rotation speed is high about 1400 rpm then a large number of the void at the SZ is formed. The void defect formation during high rotation speed in normal FSW is due to excessive heat input during welding [5-8].
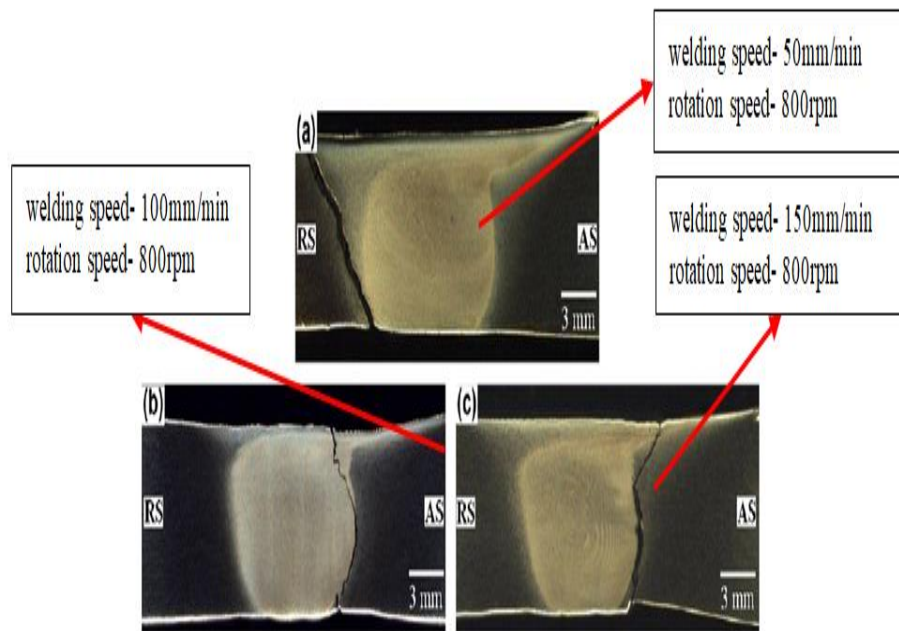

FIG.16. **Fracture locations of the joints welded at different welding speeds: (a) 50 mm/min, (b) 100 mm/min and (c) 150 mm/min.**

Along with the welding defects, the fracture features also vary significantly with the welding speed for the defect-free joint as shown in Figure 15. At a lower welding speed of 50 mm/min, the tensile specimen of the joint are all fractured in the heat-affected joint adjacent to the TMAZ on the RS as shown in Figure a, consistent with the lowest hardness region of the joint (Figure 15).

When the welding speed increases to 100-150 mm/min, the tensile specimen of both joints are all fractured in the TMAZ adjacent to the Weld Nugget Zone (WNZ) in Figure 15b, c. it is to be noted that because of the sharp interface between WNZ and TMAZ on the AS side, fracture occurred in the TMAZ on the AS instead of RS where there is no such sharp interface. Sharp interface causes a mismatch material deformation in the WNZ and the TMAZ during tensile testing. In a word, the welding speed must be chosen within an optimum range to obtain a high-quality joint through underwater friction stir welding.
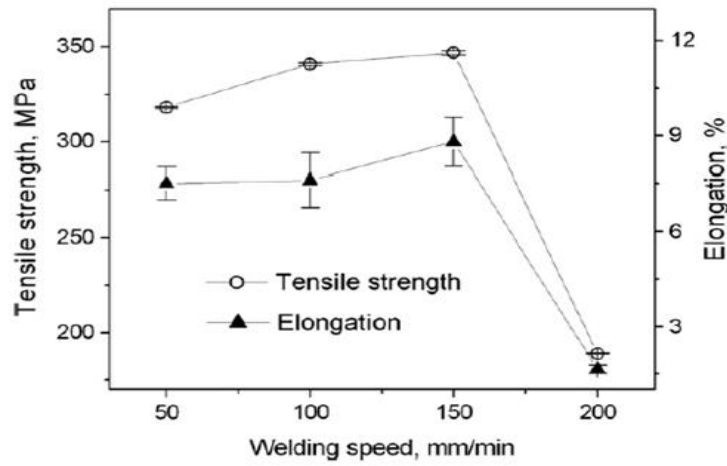
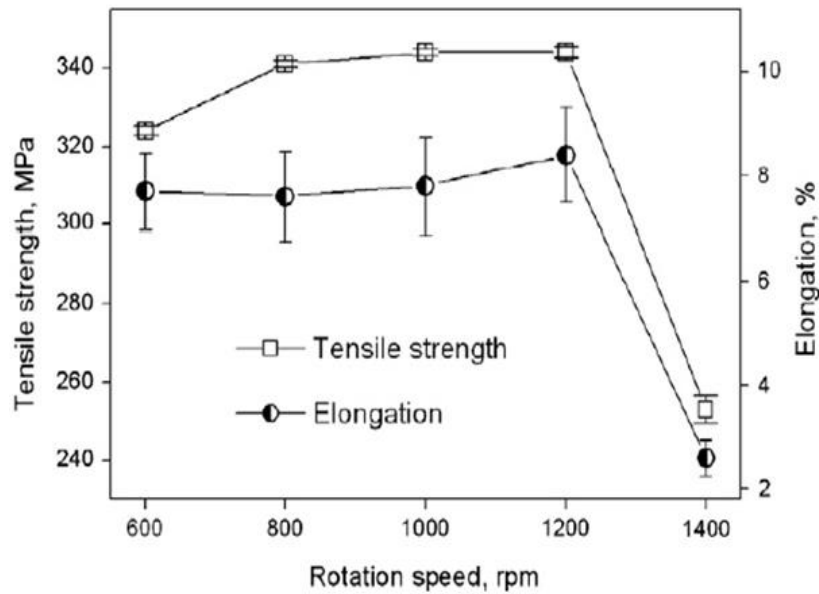FIG.17. **Tensile properties of joint at different welding speeds (Rotation speed = 800 rpm).**

FIG.18**. Tensile properties of joint at a different rotation speed (Welding speed =100mm/min).**

Figure 16 shows how a tensile property varies with welding speed and rotation speed. From the figure, it can be observed that the tensile strength continuously increases with increasing welding speed from 50-150 mm/min with a constant rotation speed of 800 rpm and reaches a maximum at 150 mm/min showing the maximum tensile strength of 347 MPa equivalents to 80% of the base metal. As we go on increasing welding speed further beyond 150 mm/min there is a drastic decrement in the tensile strength due to the coarsening and transformation of theta' precipitates which are weakened due to lower heat input. Similarly, (Figure 17) interprets the identical behavior of the tensile property as former with increasing rotation speed from 600-1200 rpm and reaches a maximum at 1200 rpm showing the maximum tensile strength of 341MPa equivalent to 80% of the BM. As we further go on increasing the rotation speed beyond 1200 rpm up to 1400 rpm the tensile strength deteriorates due to the void defect at a high rotation speed. The deterioration in the elongation behavior at a high rotation speed (beyond 1200 rpm) and high welding speed (beyond 150 mm/min) may be because of an increase in both grain size and dislocation density in the SZ [5-8].
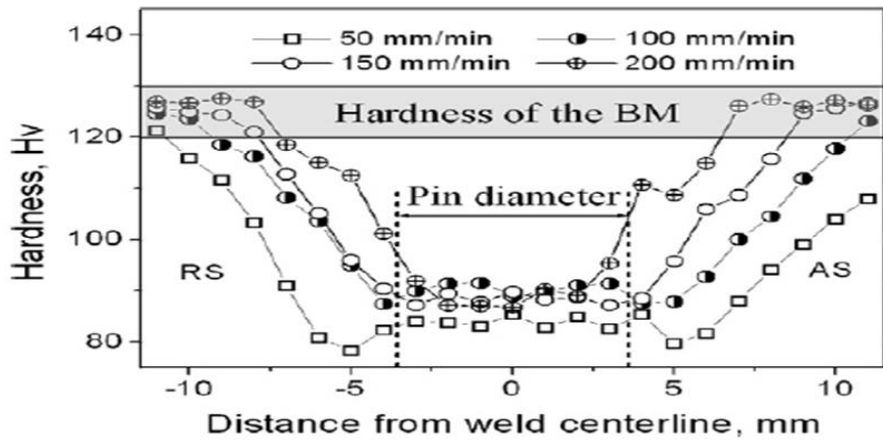
FIG.19. **Micro-hardness distributions of the joints welded at different welding speeds (Rotation speed=800 rpm).**
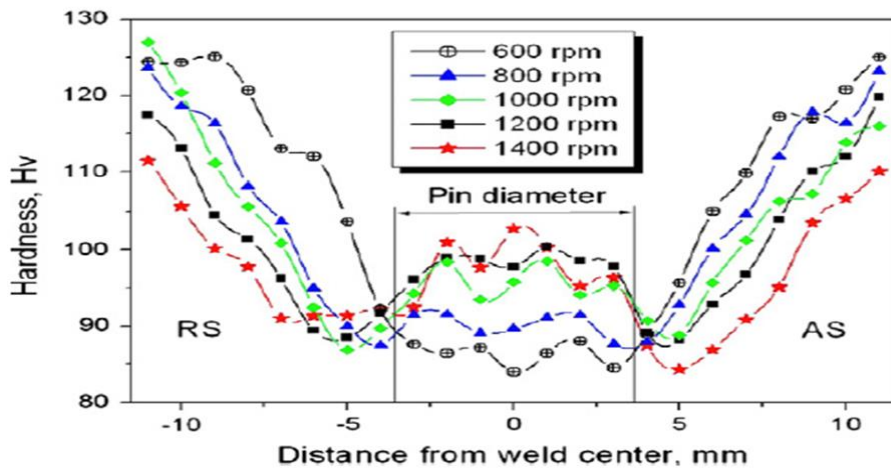

FIG.20. **Hardness profile of the joint at different rotation speeds (Welding speed =100 mm/min).**

Comparing (Figure 18) with (Figure 19), it is obvious that the defect-free joint all fail at their separate lowest hardness location, as a result, the tensile strength and hardness minimum of the joint display similar evolving trends with increasing the rotation speed. The hardness profile indicates that the softening region width increases with the increase of rotation speed suggesting an improvement in the plastic deformation ability of the joint. However, it is also to be noted that the hardness of the SZ also increases with the rotation speed, which promotes the strain hardening capacity of this zone. The synergetic effects of this two-factor allow the elongation not to change significantly from 600-1200 rpm [8]. Hence the rotation speed must be chosen in an appropriate range to produce high-quality joint through underwater FSW, as too low or too high rotation speed can both yield poor joint properties. The former owing to the inadequate tool stirring while the latter is attributed to the excessive heat input. As shown in the figure, the hardness of the thermomechanical affected zone and heat-affected zone increases with increasing welding speed, leading to a gradual narrowing of the softening region. This may be due to the weakening of precipitate deterioration in the two regions as the welding speed increases. The lowest hardness of the joint welded at 50 mm/min is located in the HAZ adjacent to the TMAZ on the RS. When the welding speed increases to 100-150 mm/min. the lowest hardness is at the TMAZ adjacent to the WNZ on either side of the weld. For the joint welded at 200 mm/min, the lowest hardness is lying in the WNZ. Hence we can say that the lowest hardness region of the joint move towards the weld center with increasing the welding speeds. Furthermore, the lowest hardness value increases with the welding speed due to the precipitate deterioration level at the weakest location of the joint (Figure 20) [5-8].
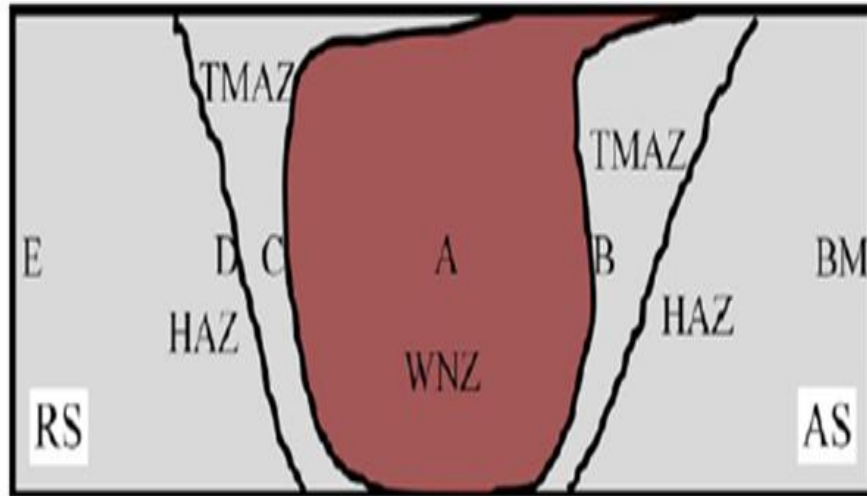
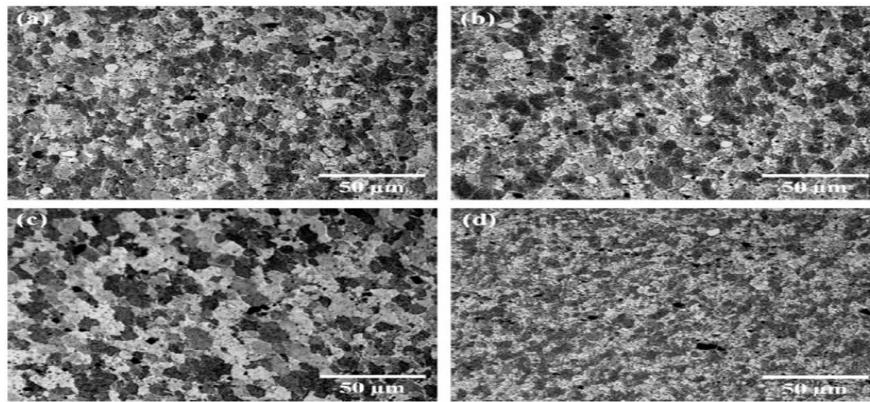FIG.21. **The schematic view of exact locations where microstructural analyses is performed.**

FIG.22. **Grained structures of the WNZ formed at different welding speeds: (a) 50 mm/min, (b) 100 mm/min, (c) 150 mm/min and (d) 200 mm/min.**
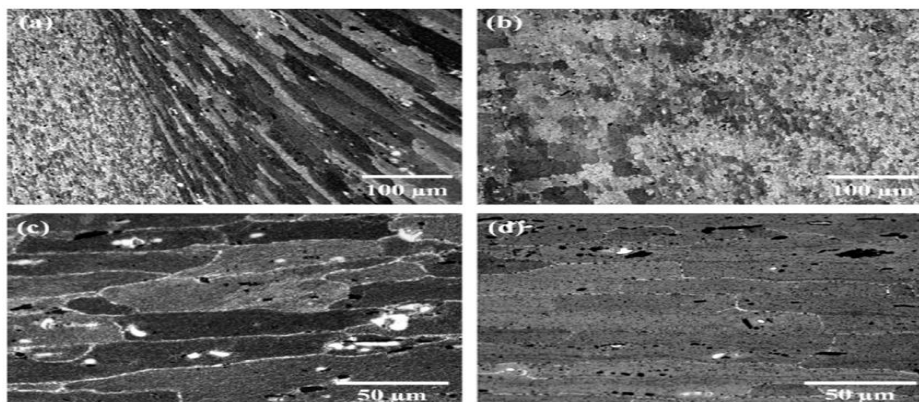

FIG.23. **Representative grained structures of the TMAZ, the HAZ, and the BM (obtained at 150 mm/min): (a) TMAZ on the AS, (b) TMAZ on the RS, (c) HAZ, and (d) BM.**

In Figure 21 the fine equiaxed grains due to the dynamic recrystallization during underwater FSW. The welding speed has a significant effect on the grain size. As the welding speed increases from 50-200 mm/min (Figure 22), the average grain size of the refined grain is determined to be 6.8 μm, 7.5 μm, 10 μm, and 2.5 μm respectively by the mean linear intercept method. Here it is observed that the grain size firstly increases from 50-150 mm/min and then decreases to a very low value at 200 mm/min. This evolving trend of grain size with welding speed may result from the synergetic effects of the material deformation and heat input during underwater FSW. As the welding speed increases it results in a decrease in both the degree of material deformation and the heat input during underwater FSW. The decrease in the degree of material deformation generally leads to an increase in the recrystallized grain size [8] while the decrease in heat input tends to result in grain refinement. Therefore the variation of grain size with welding speed depends on which factor is dominant. It seems that the material deformation mainly controls the grain size at welding speed lower than 150 mm/min. At a relatively high welding speed of 200 mm/min, it is the heat input that dominates the final grain size.

In the figure, a little variation in grain structure can be observed with the increase in welding speed in the TMAZ and HAZ. The grains are highly extruded and elongated in the TMAZ on the AS, which creates a sharper interface between the WNZ and the TMAX. This is in contrast with the RS of the weld, where the WNZ/TMAZ interface is rather unclear. The HAZ only experiences welding thermal cycles and no plastic deformation occurs in this region during the underwater FSW, as a result, the heat-affected zone shows a similar grained structure to the base metal (Table 11) [8].

7055-T6 Aluminum alloy

TABLE 11. **Welding parameter of experiments.**

| Chemical composition %		Group	Number	Welding parameter		Remark
Al	Bal.			Traveling speed (mm/min)	Rotation speed (rpm)	
Zn	8.00					
Mg	2.10	S	1		750	Fixed high traveling speed, different rotation speed
Cu	2.30		2	155	1050	
Mn	0.05		3		1550	
Cr	0.04		4		3000	
Fe	0.15	F	1	155		Fixed low rotation speed, different traveling speed
Si	0.10		2	105	750	
Ti	0.06		3	75		
		F'	1	75		Fixed high rotation speed, different traveling speed
			2	155	1550	
			3	300		
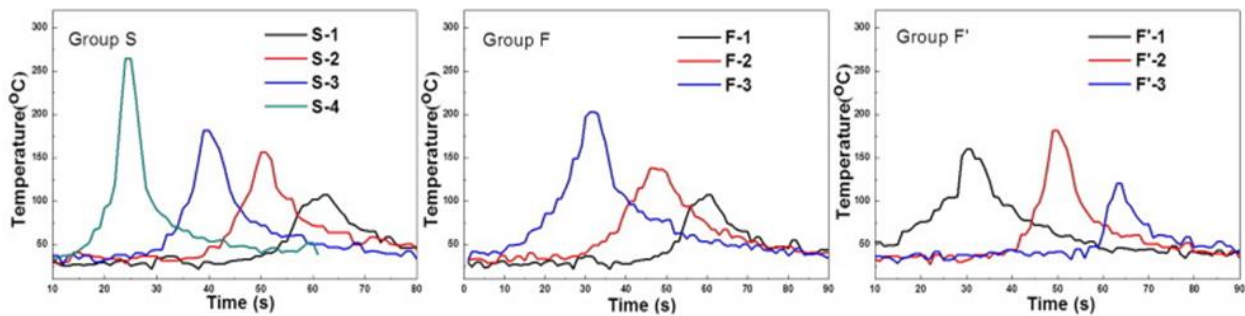
FIG.24. **Thermal cycles.**

The thermal cycle of the joint has a significant effect on the heat generation and heat dissipation of underwater weld. A high rotation speed, on one hand, increases the fraction of heat of the material, on the other hand, speeds up the circulation of water

and accelerates the heat dissipation which leads to a high cooling rate. Though a high traveling speed may bring more deformation heat, the increase in traveling speed also makes a shorter duration time of heat, and the water environment accelerates the cooling process. So, high traveling speed may lead to a low-temperature thermal cycle [9].

Figure 23 shows the comparison of thermal cycles of three groups and their characteristics value is listed in the table below. The residence time means the duration that the temperature of the workpiece is above 45°C and the cooling rate is calculated by the formula of peak temperature (°C)/cooling time (s). The parameter design in each group is settled by fold change in rotation speed (group S) or traveling speed (group F and F') [9].

Microstructure: As shown in Figure 24 at a low rotation speed (S-1, 750 rpm), the weld joint has a huge furrow defect which reveals an insufficient flow of metal during the welding process and distinct onion ring character. When rotation speed increases to 1050 rpm (S-2) the furrow defect is healed and the weld nugget becomes uniform without an onion ring. With a further increase of rotation speed to 1550 rpm (S-3), the appearance is perfectly smooth and the weld nugget is full. Under the rotation speed of 3000 rpm (S-4), the appearance of the joint becomes rough containing some burrs which indicate overheating of the joint [9].

Figure 25 shows the weld of group F. the furrow defect in F-1 (S-1) can also be reduced by decreasing the traveling speed. At a traveling speed of 105 mm/min (F-2), the furrow defect is replaced by a tunnel defect on the AS. With a further decrease in traveling speed to 75 mm/min (F-3), a defect-free joint is obtained finally. However, it will lead to a decline in production efficiency.

The appearances of weld in group F' get brighter and smoother from F'-1 to F'-3 as shown in Figure 26. When the traveling speed is 75 mm/min (F'-1) the joint is integrity as a whole but a kissing bond defect (S line). It is due to the longer time of heat because of low traveling speed which prompts a reaction of oxygen in the water and weld metal than the "S line" is introduced. This "S line" is eliminated in F'-2 parameters with higher traveling speed and shorter duration time of heat. On further increasing the traveling speed to 300 mm/min (F'-3) a huge tunnel defect is left in the center bias of the AS. The plastic flow metal gets rapidly cooled in an underwater environment and is unable to fill the weld before its solidification [9].
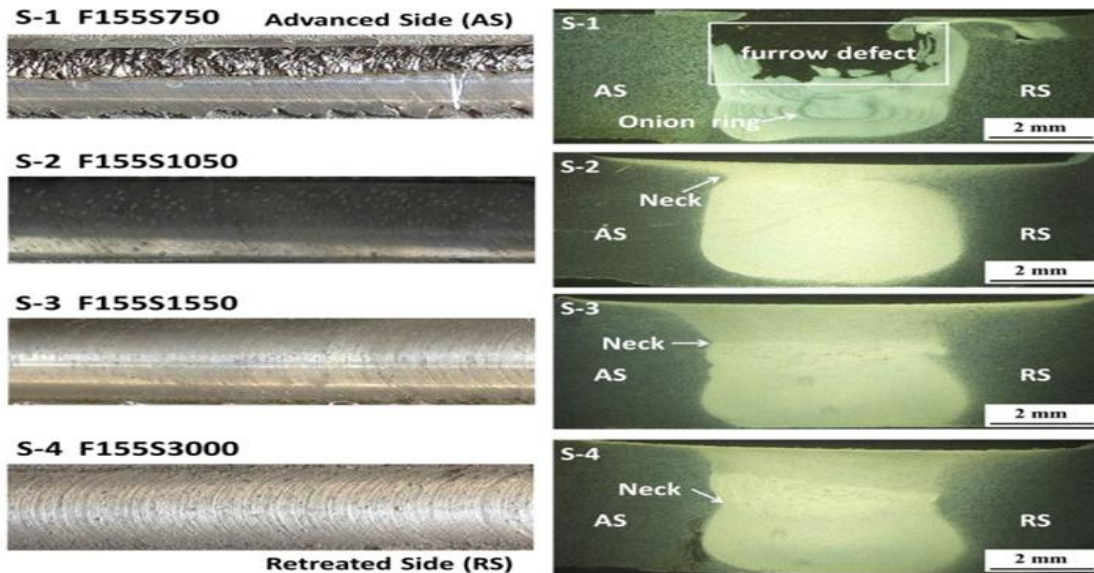

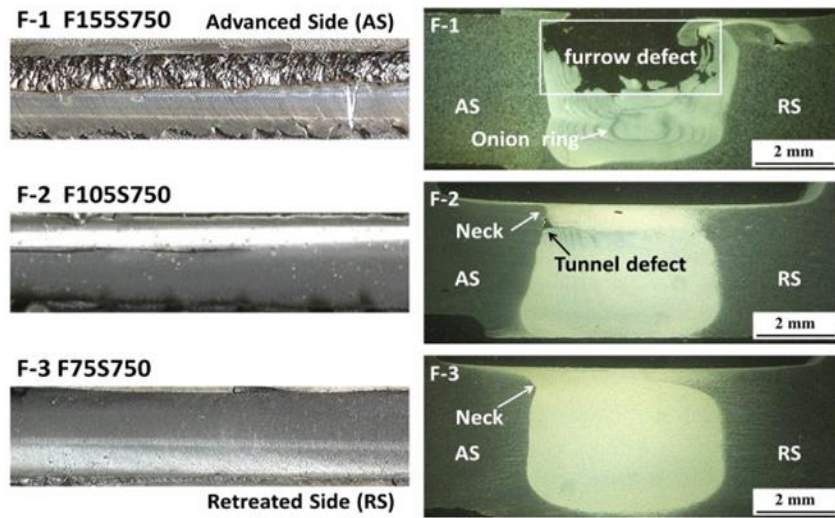FIG.25. **Appearances of welds of group F.**
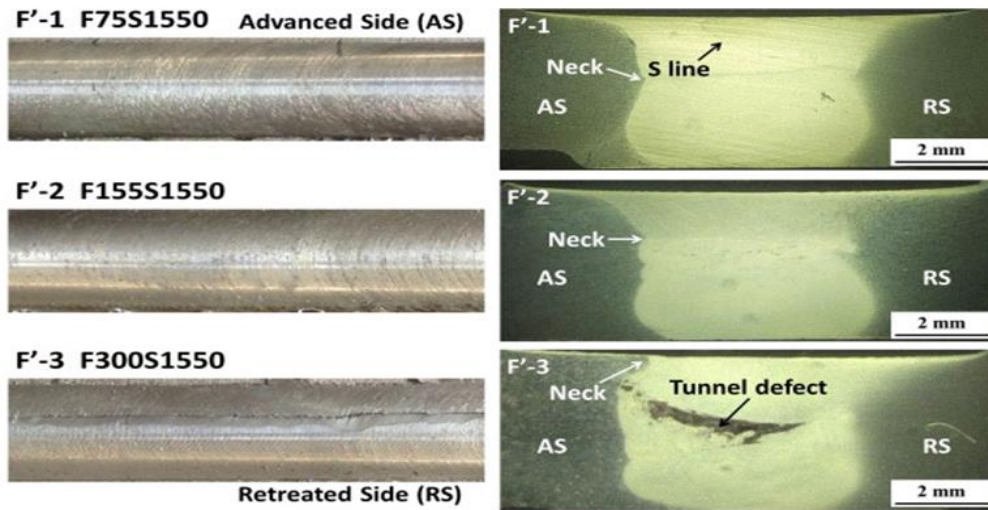
FIG.26. **Appearances of welds of group F.**

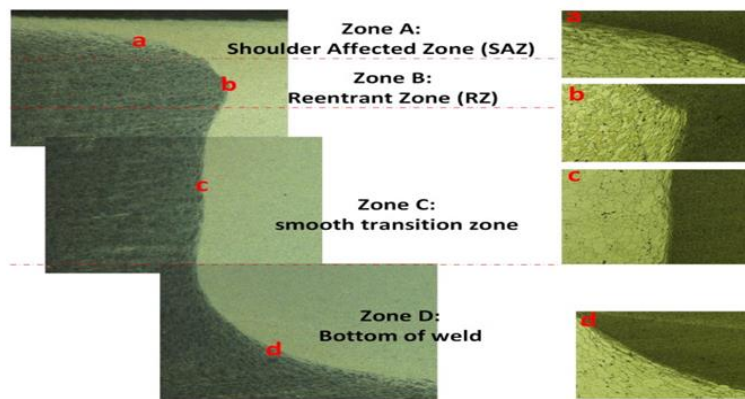FIG.27**. Appearances of welds of group F**.

FIG.28. **Illustration of districts along weld boundary.**

To depict the characters clearly, the boundary is divided into four zones as shown in Figure 27 actually, the boundary is formed by grains of different sizes and shapes, and the grains which blame for the action of the pin tool. In different zones, the variation of grains has its feature. Zone A, namely the Shoulder Affected Zone (SAZ), is characterized by recrystallization grains and grains here suffer severe deformation through the extrusion action of the shoulder of the tool pin. Zone B is named Reentrant Zone (RZ) and it is defined as the narrowest neck of the weld on the cross-section. The shape of RZ is depicted by elongated grains with the tip of the reentrant as a radial distribution center. Zone C is a smooth transition zone and on both sides of the boundary, the size of grains differs a lot. The bottom of the weld (Zone D) consists of layers of elongated grains along the boundary. Among the four zones, RZ is a hard-flow zone. The formation of RZ, especially the necks, presents a balance of heat transfer and grain deformation. In the RZ, metal needs to heal the joint, and its fluidity is determined by the remaining heat. If remained plastic flow metal fails to fill the joint, the ductile metal is dragged to make up the joint which suffers severe deformation. So the position where heat is sufficient consists of less deformation grain due to better fluidity of metal while the last area that heals, namely RZ, usually contains the most severe deformation and mixed microstructure. Also, if the deformation still can't remedy the loss of metal, tunnel defect tends to occur at the tip of RZ on the advanced side. So the RZs of the advanced side are compared in this study [9].

Tensile test: From Figure 28 we can observe that the tensile strength goes on increasing in the S group as the rotation speed increases from S-1 to S-4. The minimal value of tensile strength for S-1 may be attributed to the furrow defect which brought fracture at a lower strength. With increasing rotation speed to S-2, the furrow defect healed consequently showing higher tensile strength. On the further increase of rotation speed to S-3, there is sufficient material flow to fill the weld area, as a result, a smooth and defectless joint formed showing high tensile strength which is also reflected on the even high rotation speed of 3000 rpm (S-4).

The second group also shows the same behavior of increasing tensile strength but its tensile strength increases with decreasing traveling speed. In the F group when the traveling speed is 155 mm/min the time duration for material to fill the weld joint is insufficient and the heat dissipation rate is higher as a resulting defect remains significant owing to lower tensile strength. When the traveling speed decreases to 105 mm/min or further to 75 mm/min the time duration for material to fill the weld joint is sufficient enough to heal the furrow defect and tunneling defect as a result tensile strength goes on increasing [9].

As for the F' group, the result shows a peak value at F'-2, however, when the traveling speed rises to 300 mm/min (F'-3), a huge defect left in the joint leads to an abrupt decrease in the property of joint. Hence the rotation speed and traveling speed should be matched carefully otherwise it will lead to serious defects in the joint.
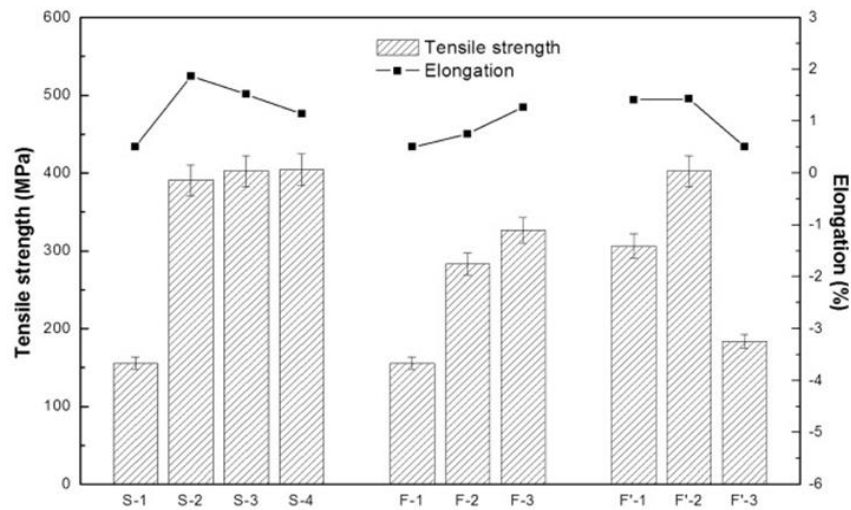

FIG.29. **Results of tensile test [9].**

Corrosion Behavior of Aluminum Alloys

Spray formed 7055 Al alloy: When this alloy is welded using UWFSW, it will affect the corrosion behavior of the alloy. The under-water joint is characterized by a typical pattern of inter-granular corrosion that its corrosion path was not along the grain boundary. High potential phase $MgCu_2$ contributes to the traditional joint blocked corrosion process to some extent but the non-uniform distribution of $MgCu_2$ leads to a weak zone for corrosion. UWFSW is better than traditional joint as it suppresses the formation of $MgCu_2$ and enlarges the quantity of efficient strengthening particle $MgZn_2$. Due to the discontinuous path corrosion process was blocked so it performed better resistance to corrosion. At the same time, UWFSW is prone to Exfoliation corrosion. The exfoliation corrosion was a special type of IGC. When corrosion products dissolved in corrosive solution, a vacancy was left in the position of the grain boundary that led to wedge-shaped tensile stress. With the increasing corrosion time, the stress accumulated between grain and grain boundary. Once the tensile stress reached a threshold value that was large enough to make the upper grains depart from the inner gains, the number of grains would peel off along with corrosion products then exfoliation corrosion went on continuously.
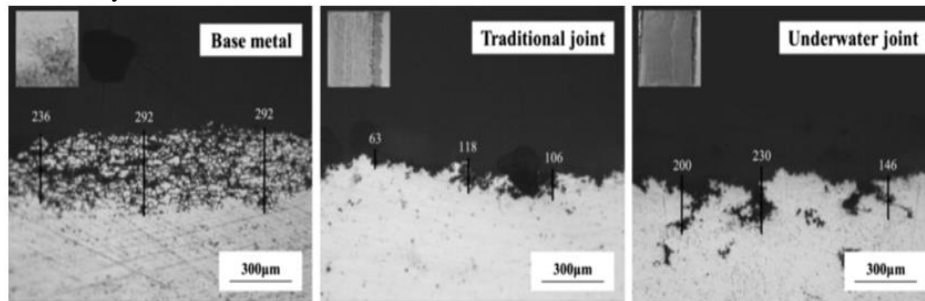

FIG.30. **Appearance of IGC samples in cross-section and measurement for corrosion depths.**

From Figure 29 we can conclude that corrosion depth for UWFSW is less than base metal but more than a traditional joint. In the base metal, the Inter-Granular Corrosion (IGC) is of the form of a thick reticular pattern and along the grain boundary while in FSW and UWFSW the IGC consists of corrosion pits. The corrosion pit of FSW is shallow attributing surface irregularity. In UWFSW the pits are deep with ambiguous corrosion paths.

Residual stresses in UWFSW of aluminum alloys

T6 aluminum alloy: RS caused by FSW and UWFSW is examined using the non-destructive ultrasonic method for aluminum AA7075-T6. The impact of the cooling media, as well as welding velocities on both longitudinal and transverse RS, is indispensable. Nevertheless, all of them correlate with RS through the temperature rise and applied forces, each of which exhibits dominating impact on the extension of the RS. The thermo-mechanical RS, as clear from its name, is only the result of the combination between the thermal field and mechanical stresses induced on the workpiece, which is correlated with temperature distribution and mechanical forces applied by the FSW tool on the work-piece, respectively. Meanwhile, throughout the FSW process, the induced mechanical and thermal stresses exhibit a close correlation. On one hand, the applied forces by the FSW tool directly affect the heat generated *via* the FSW tool and consequently the temperature distribution as well as the corresponding thermal stresses. On the other hand, the higher the temperature, the lower the yield strength. Thus, the higher temperature leads to more softening and consequently less resistance of the material against the FSW tool. Therefore, it is expected that as the temperature increases, lower forces are applied to the workpiece by the FSW tool and vice versa. Thus, both the mechanical and thermal aspects should be concurrently taken into account to provide a better understanding of the RS caused by the FSW process. The translational and axial forces increase dramatically when the cooling media changes from air to water. Such a dramatic increase can be attributed to the reduction in softening of the material around the tool due to a considerable reduction in the temperature rise [14, 1-3]. Lower temperature rises and smoother thermal gradient over the work-piece can lead to lower induced RS and on the other hand, the greater forces applied on the work-piece may lead to higher RS.

As it is evident from Figure 30, regarding the FSW in the open air, the RS considerably decreases when water is used as the surrounding fluid. The highest level of reduction in the longitudinal RS occurs within the nugget zone (17 %) while the reduction in the transverse RS reaches even 70 % within the HAZ. Therefore, it is observed that the RS caused by underwater FSW is considerably lower than air. Thus, regarding the aforementioned observations and discussion, since that portion of the RS, corresponding to the thermal field, in contrast to that portion, corresponding to the applied mechanical forces, is lower for underwater FSW than in open-air FSW, the temperature field may exhibit more dominating impact on the RS compared to the applied mechanical forces [14, 1-3].

Based on Figure 31 a, b, it is evident that under both cooling media, the RS is greater on the advancing side as compared to the retreating side, which can be attributed to the higher temperature rise as well as more severe plastic deformation. It is worth noting that, contrary to the retreating side, the traverse and rotation velocities of the materials beneath the shoulder are in the same direction leading to higher velocity as well as deformation of the plasticized materials and consequently higher temperature gradient and induced stresses are expected. Coupled with this, two more common behaviors are also observed in Figure 30. According to Figure 30, the longitudinal RS in both water and air is about four times greater than the transverse RS. It should be noted that the longitudinal RS is of tensile and compressive states inside and outside of the nugget zones, respectively. It is of great importance when the welds are operationally subjected to cyclic loading, in which the tensile RS may accelerate the crack growth while the compressive RS can commonly resist the crack growth and consequently extend the structure lifetime.
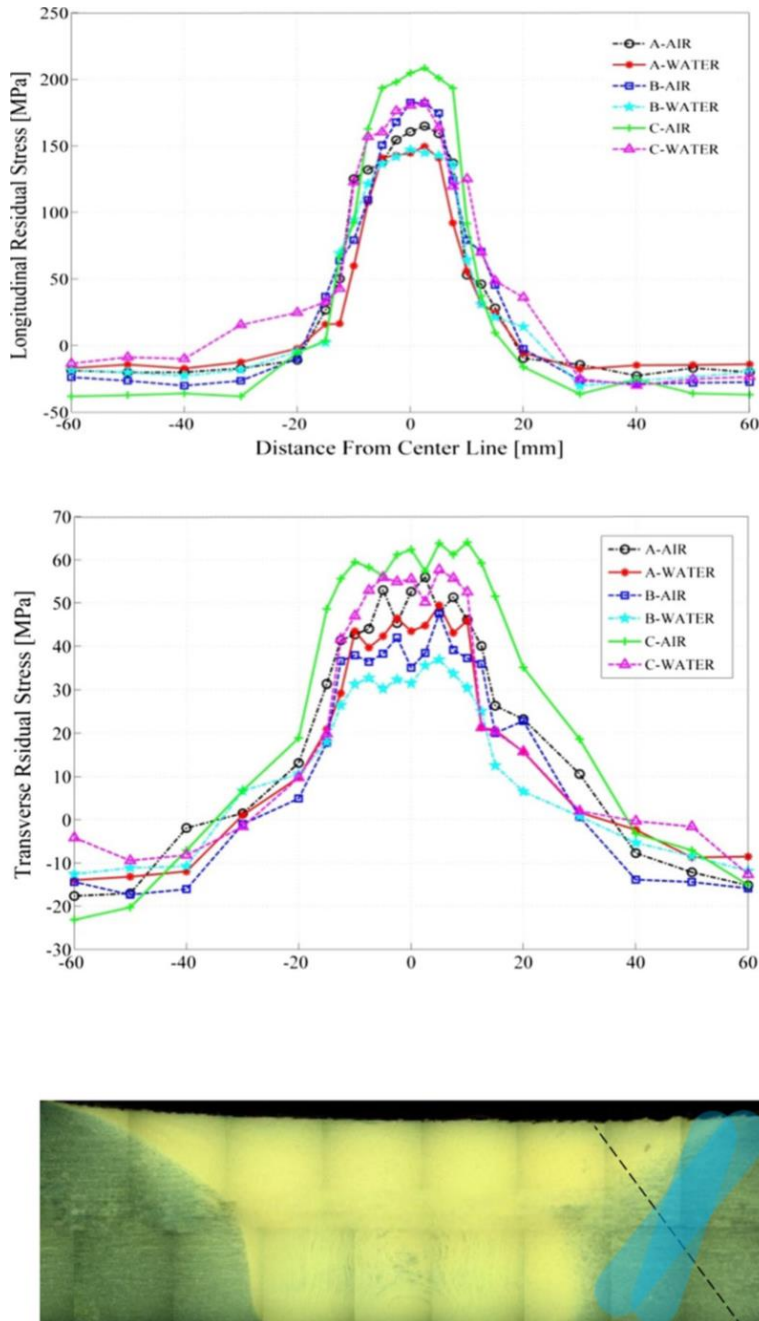

FIG 31: **Measured residual stresses based on the center line (a) Longitudinal RS and (b) transverse RS.**

Conclusion

Water media can reduce the longitudinal residual stresses down to 82% in the nugget zone. Residual stress reduction along the longitudinal direction, arising from using water, is more considerable than that along the transverse direction. The residual stresses in the longitudinal direction are four times larger than that in the transverse direction for both air and water media. The longitudinal residual stress is tensile inside the nugget zone; however, outside this zone, the residual stress is compressive for both air and water media. The residual stress is about 17% greater on the advancing side as compared to the retreating side. The effect of temperature on the residual stress induced through the friction stir welding is more dominating than the mechanical forces applied to the materials through the tool. Although the effect of residual stresses on the cyclic strength may be undeniable, in this study, residual stresses did not exhibit a considerable impact on the static strength of the defects-free welds obtained *via* FSW in both air and water.

References

1. Mishra RS, Ma ZY. Friction stirs welding and processing. Mater Sci Eng: R: Reports. 2005;50(1-2):1-78.
2. KI Mori, Y Abe. A review on mechanical joining of aluminium and high strength steel sheets by plastic deformation. Int J Lightweight Mat Manuf. 2018; 1(1):1.
3. J Ahn, E He, L Chen, et al. In-situ micro-tensile testing of AA2024-T3 fibre laser welds with digital image correlation as a function of welding speed. Int J Lightweight Mat Manuf. 2018;1(3):179e188.
4. Rajakumar S, Muralidharan C, Balasubramanian V, et al. Establishing empirical relationships to predict grain size and tensile strength of friction stir welded AA 6061-T6 aluminium alloy joints. Trans Nonferrous Met Soc. 2010; 20:1863-1872.
5. Rathinasuriyan C, Senthil Kumar VS, Shanbhag AV, et al. Radiography and Corrosion Analysis of Sub-merged Friction Stir Welding of AA6061-T6 alloy. Procedia Eng. 2014;97:810-818.
6. Lokesh R, Senthil Kumar VS, Rathinasuriyan C, et al. Optimization of process parameters: Tool pin profile, rotational speed and welding speed for submerged friction stir welding of AA6063 alloy. Int J Tech Res. 2015; 12:35-38.
7. F Gao, Q Gao, P Jiang, et al. Microstructure and mechanical properties of Ti6321 alloy welded joint by EBW. Int J Lightweight Mat Manuf. 2018;1(4):265-269.
8. L Chen, YN Hu, EG He, et al. Microstructural and failure mechanism of laser welded 2A97 AleLi alloys *via* synchrotron 3D tomography. Int J Lightweight Mat Manuf. 2018;1(3):169-178.
9. Zhang J, Shen Y, Yao X, et al. Investigation on dissimilar underwater friction stir lap welding of 6061-T6 aluminium alloy to pure copper. Mater Des 2014; 64:74-80.
10. Wang Q, Zhao Y, Yan K, et al. Corrosion behaviour of spray formed 7055 aluminium alloy joint welded by underwater friction stir welding. Mater Des. 2015; 68:97-103.
11. Zhang H, Liu H. Characteristics and formation mechanisms of welding defects in underwater friction stir welded aluminium alloy. Metallogr Microstruct Anal. 2012: 1(6):269-281.
12. M Hassan, A Ali, M Ilyas, et al. Experimental and numerical simulation of Steel/Steel (St/St) interface in bi-layer sheet metal. Int J Lightweight Mat Manuf. 2019;2:89-96.
13. S Rajakumar, C Muralidharan, V Balbasubramanian, et al. Predicting tensile strength, hardness and corrosion rate of friction stir welded AA6061-T6 aluminium alloy joints. Mater Des. 2011;32: 2878-2890.
14. Rathinasuriyan C, Senthil Kumar VS. Submerged Friction Stir Welding and Processing: Insights of Other Researchers. Int J Appl Eng Res. 2015;10(8):6530-6536.
15. Su H, Wu CS, Pittner A, et al. Simultaneous measurement of tool torque, traverse force and axial force in friction stir welding. J Manuf Process. 2013;15(4):495-500.
16. K Elangovan, V Balasubramanian, M Vallipan, et al. Influences of tool pin profile and axial force on the formation of friction stir processing zone in AA6061 aluminium alloy. Int J Adv Manuf Technol. 2008; 38:285-295.
17. K. Elangovan, V. Balasubramanian, S. Babu. Predicting tensile strength of friction stir welded AA6061 aluminium alloy joints. Mater Des. 2009; 30:188-193.

18. Jonckheere C, de Meester B, Denquin A, Simar A. Torque, temperature and hardening precipitation evolution in dissimilar friction stir welds between 6061-T6 and 2014-T6 aluminium alloys. J Mater Process Technol. 2013; 213(6):826-837.

19. El-Hafez HB. Mechanical Properties and Welding Power of Friction Stirred AA2024-T35 Joints. J Mater Eng Perform. 2011; 20(6):839-845.

20. WM Zeng, HL Wu, J Zhang, et al. Effect of tool wear on microstructure, mechanical properties and acoustic emission of friction stir welded 6061 Al alloys. Acta Metall Sin. 2006; 19(1): 9-19.